AD-A098 237 OREGON STATE UNIV CORVALLIS DEPT OF ATMOSPHERIC SCIENCES F/G 20/4
DEPENDENCE OF MIXED-LAYER ENTRAINMENT ON SHEAR STRESS AND VELOC--ETC(U)
APR 81 J W DEARDORFF, G E WILLIS N00014-79-C-0440

UNCLASSIFIED NL

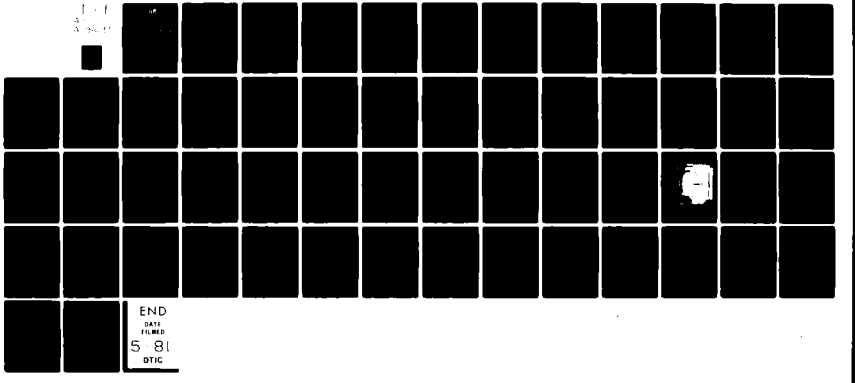

END
DATE FILMED
5 81
DTIC

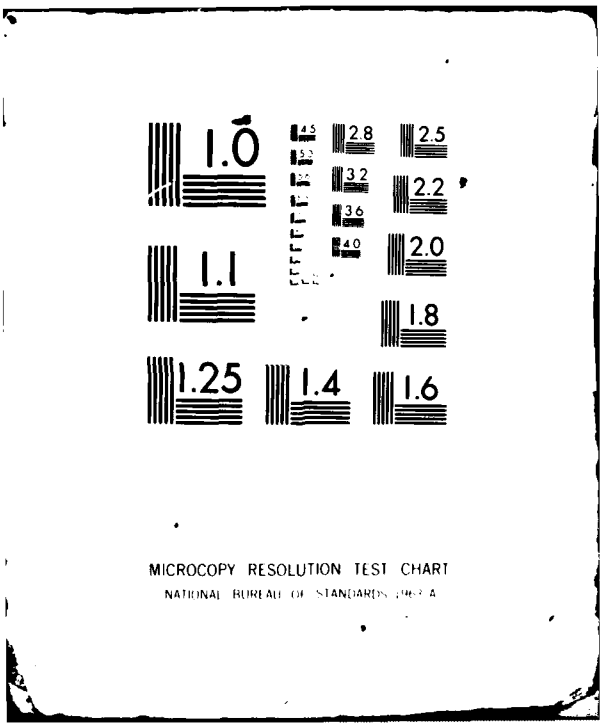
1.0
1.1
1.25
1.4
1.6
1.8
2.0
2.2
2.5
2.8
3.2
3.6
4.0
4.5
5.0
MICROCOPY RESOLUTION TEST CHART
NATIONAL BUREAU OF STANDARDS 1963-A

Contractor Report
N00014-79-C-0440-1

LEVEL II

12

AD A098237

DEPENDENCE OF MIXED-LAYER ENTRAINMENT ON SHEAR STRESS AND VELOCITY JUMP

Prepared By:

J. W. Deardorff and G. E. Willis

Department of Atmospheric Sciences
Oregon State University
Corvallis, Oregon 97331

APRIL 1981

Final Report for Period 1 May 1979 - 30 April 1981

Contract No. N00014-79-C-0440

Prepared For:

Fluid Dynamics Program, Code 438
Office of Naval Research
800 N. Quincy St.
Arlington, Virginia 22217

UNCLASSIFIED

SECURITY CLASSIFICATION OF THIS PAGE (When Data Entered)

REPORT DOCUMENTATION PAGE

READ INSTRUCTIONS BEFORE COMPLETING FORM

1. REPORT NUMBER: N00014-79-C-0440-1
2. GOVT ACCESSION NO.: AD-A098237
3. RECIPIENT'S CATALOG NUMBER: rept.

4. TITLE (and Subtitle): Dependence of Mixed-Layer Entrainment on Shear Stress and Velocity Jump.

5. TYPE OF REPORT & PERIOD COVERED: Final, 1 May 1979 - 30 Apr 1981

6. PERFORMING ORG. REPORT NUMBER

7. AUTHOR(s): J. W. Deardorff and G. E. Willis

8. CONTRACT OR GRANT NUMBER(s): N00014-79-C-0440

9. PERFORMING ORGANIZATION NAME AND ADDRESS:
Department of Atmospheric Sciences
Oregon State University
Corvallis, OR 97731

10. PROGRAM ELEMENT, PROJECT, TASK AREA & WORK UNIT NUMBERS: Task NR 062-640

11. CONTROLLING OFFICE NAME AND ADDRESS:
Fluid Dynamics Program, Code 438
Office of Naval Research
Arlington, VA 22217

12. REPORT DATE: 30 Apr 1981

13. NUMBER OF PAGES: 55

14. MONITORING AGENCY NAME & ADDRESS (if different from Controlling Office)

15. SECURITY CLASS. (of this report): Unclassified

15a. DECLASSIFICATION/DOWNGRADING SCHEDULE

16. DISTRIBUTION STATEMENT (of this Report)

Approved for public release; distribution unlimited.

17. DISTRIBUTION STATEMENT (of the abstract entered in Block 20, if different from Report)

18. SUPPLEMENTARY NOTES

Preprint to be published in J. Fluid Mech. in 1981 or 1982.

19. KEY WORDS (Continue on reverse side if necessary and identify by block number)

Mixed-Layer Growth
Annulus Experiments
Entrainment
Shear-induced Turbulence

20. ABSTRACT (Continue on reverse side if necessary and identify by block number)

From new rotating-screen annulus experiments, the mixed-layer growth rate is found to depend on both the surface friction velocity and the interfacial velocity jump in a multiplicative sense, with the velocity-jump dependence being the stronger. The dimensionless velocity-jump parameter, R_v, can vary substantially during entrainment. The effect of sidewall friction, if not too strong, is to decrease the entrainment rate through its increase of R_v.

(Detailed abstract on next page)

DD FORM 1 JAN 73 1473 EDITION OF 1 NOV 65 IS OBSOLETE
S/N 0102-LF-014-6601

411090

UNCLASSIFIED

SECURITY CLASSIFICATION OF THIS PAGE (When Data Entered)

PREPRINT

DEPENDENCE OF MIXED-LAYER ENTRAINMENT ON SHEAR STRESS AND VELOCITY JUMP

ABSTRACT

From rotating-screen annulus experiments the entrainment rate, w_e, normalized by the friction velocity, u_*, has been found to be a function of both the overall Richardson number, R_τ, and the inverse Froude number, R_v. The $R_\tau^{-\frac{1}{2}}$ dependence deduced by Price (1979) and Thompson (1979) satisfactorily explains the present data if multiplied by an approximate $R_v^{-1.4}$ dependence. The measurements indicate that R_v is a variable that is influenced by sidewall friction, time after onset of the surface stress, or other factors. The greater w_e/u_* values of the Kantha et al. (1977) type experiment over that of the Kato & Phillips (1969) experiment can be explained by somewhat greater R_v values in the latter case.

A close connection is now apparent between entrainment experiments in two-layer systems designed to have only one velocity scale (the interfacial velocity jump, Δv), and the rotating-screen annulus experiments having two velocity scales (u_* and Δv). The former also have (at least) two velocity scales, the second one being associated with the presence of turbulence throughout one or both of the fluid layers.

The turbulent layer is found to be quite well mixed in density only if w_e/u_* does not exceed about 0.03, or $w_e/|\Delta v|$ does not exceed about 0.003. The present data suggest more rapid entrainment when temperature rather than salt provides the density jump, as first noted by Turner (1968) in oscillating grid experiments. If this is a Peclet number effect, the trend did not continue for still much greater Pe values, the data for kaolin (clay) being very compatible with that for salt.

1. Introduction

The rate at which a well mixed turbulent layer entrains an adjacent non-turbulent layer in geophysically relevant situations is believed to depend upon the surface shear stress, $\underline{\tau}$, the depth of the mixed layer, h, and the buoyancy jump b across the edge of the layer ($b = g|\Delta\rho|/\rho_o$, where g is the gravitational acceleration, ρ_o a reference density of one of the layers, and $\Delta\rho$ the change in density across the outer edge of the mixed layer). If a surface flux of buoyancy or heat is present, that quantity may also be important; however here only the problem of the neutral surface layer driven by shear stress will be considered.

The first set of experiments undertaken to explore the dependence of the growth of a neutral mixed layer upon these factors was that of Kato and Phillips (1969, abbreviated KP) using an annulus of diameter 1.52m and gap $\Delta r = 0.23$m. The approximate relation they found is

$$w_e/u_* = 2.5\ R_\tau^{-1} \tag{1}$$

where w_e is the entrainment rate, or mixed-layer growth rate, u_* is the friction velocity $(|\underline{\tau}|/\rho_o)^{\frac{1}{2}}$, and

$$R_\tau = bh/u_*^2 \tag{2}$$

is an overall Richardson number. Their actual data suggested a power law somewhat less steep than R_τ^{-1} at small R_τ values ($R_\tau < 50$) and somewhat steeper at larger values ($R_\tau > 100$). In their experiments, using a turbulent layer of fresh water (driven by a rotating screen) overlying a non-turbulent linearly stratified outer layer (abbreviated SOL) of salt solution, u_* was obtained directly from torque measurements; however, quantitative velocity measurements were not made.

Later, using the same annulus, Kantha et al. (1977, abbreviated KPA) explored the two-layer system (abbreviated 2LS) in which the non-turbulent lower layer is denser than the turbulent upper layer but is not stratified. The entrainment rate was not found to obey any simple power-law dependence upon R_τ; values of w_e/u_*

were about half those found by KP for the same values of R_τ and $h/\Delta r$ (Price, 1979). A significant reduction in w_e/u_* with increased sidewall drag (increased $h/\Delta r$) was noted.

Soon thereafter further experiments with the 2LS were conducted by Kantha (1978) using a scaled-down annulus half as large as that of KP and KPA. His w_e/u_* versus R_τ values closely resembled those of KPA but were substantially smaller ($h/\Delta r$ was generally larger). Salinity profiles were also measured, and indicate, surprisingly, that the turbulent layer often was not very well mixed in salt content. Although the purpose of employing a smaller annulus was to determine if centrifugal effects were important, it was not clear if differences observed were associated with such effects or with generally larger sidewall drag. Near the inner annulus wall, for $R_\tau > 100$, centrifugal effects were apparently suppressing the turbulence, judging from shadowgraph observations.

An explanation for the discrepancy between the SOL and 2LS results was provided by Price (1979) and Thompson (1979). Price started with the momentum budget for the mixed layer, neglecting centrifugal effects and curvature:

$$\frac{\partial}{\partial t}(h\bar{v}) = u_*^2 - 2C_{DW}\bar{v}^2 h/\Delta r \qquad (3)$$

where $\bar{v}$ is the mean flow speed within the mixed layer and C_{DW} is the sidewall drag coefficient. Here, h is the depth of the assumed well mixed layer, which may be considerably smaller than the maximum depth reached by the mixed layer locally at any given time. Although (3) is most easily derived using the Boussinesq approximation and incompressibility condition, it can be shown to hold with equal accuracy even when the complete continuity equation is employed. Introducing the R_v notation:

$$R_v = bh/(\Delta v)^2 \qquad (4)$$

where Δv is the velocity jump across the edge of the mixed layer in the vicinity of z=h, Price transformed (3) into

$$\frac{\partial}{\partial t} R_v = \frac{2}{n} \frac{w_e}{h} R_v + 4C_{DW} \frac{u_*}{\Delta r} R_\tau^{\frac{1}{2}} R_v^{\frac{1}{2}} - 2 \frac{u_*}{h} R_\tau^{-\frac{1}{2}} R_v^{3/2} \tag{5}$$

where it was shown from the mass budget that

$$n = \begin{cases} \frac{1}{2} & \text{(SOL)} \\ 1 & \text{(2LS)} \end{cases} \tag{6}$$

In deriving (5), $|\Delta v|$ in (4) was assumed equal to $\bar{v}$ in (3) for the experimental studies that were of immediate interest. Price then assumed that

$$R_v = \text{constant} \tag{7}$$

which can be likened to a critical Richardson number across the Δv layer always being attained. With this assumption, (5) became an entrainment relation:

$$w_e/u_* = nR_v^{\frac{1}{2}} R_\tau^{-\frac{1}{2}} (1 - 2C_{DW} R_v^{-1} R_\tau h/\Delta r) \quad . \tag{8}$$

The implication is that w_e/u_* should be two times larger with the 2LS configuration than with the SOL, for a given R_τ, in close agreement with the observations. Thompson (1979) obtained the same result independently, and had already used (7) in the theory of Pollard *et al.* (1973); both stressed the importance of sidewall drag in limiting the flow speeds induced by the rotating screen and in causing w_e/u_* to decrease more rapidly than $R_\tau^{-\frac{1}{2}}$ as $h/\Delta r$ became appreciable. The value deduced for R_v was in the vicinity of 0.6.

The present study was motivated by the desire to determine in future studies how the entrainment rate is modified by the presence of a destabilizing buoyancy flux, F_b, at the surface when a surface shear stress and a velocity jump across $z=h$ are also present. The limiting case would be free convection in the absence of u_* and Δv, for which $R_v = \infty$. An alternate configuration also producing $R_v = \infty$ involves the use of an oscillating grid rather than a rotating screen to generate the turbulent boundary layer. If R_v can increase from 0.6 to ∞ by substitution of a different mechanism of turbulent mixing, it could lie anywhere in between these two limits if all three mechanisms were present to maintain the turbulence. It

may therefore be questioned if R_v is sufficiently constant, during entrainment that is driven by 2 of these 3 mechanisms (u_* and Δv), for (8) to be valid. To check this possibility requires entrainment measurements in which Δv is measured.

Assumption (7) has also been challenged by Kantha (1978) who utilized the model $w_e/u_* \propto R_\tau^{-\frac{1}{2}} R_v^{-\frac{1}{2}}$, with R_v being allowed to vary.

Another reason for desiring to check (8) is that in geophysical situations the C_{DW} term will be absent, yet a similar equation based on assumption (7) (e.g. see Pollard et al.) could be derived in which other forces would appear that could tend to alter Δv; i.e., the horizontal pressure gradient and coriolis forces. Thus (8) would then imply that large-scale forces, which may cause Δv to change slowly with time, would directly affect the entrainment rate. This contrasts with the usual viewpoint that only parameters appearing in the turbulence kinetic energy (TKE) equation, or closely allied parameters, affect the entrainment rate (e.g., see Price et al., 1978). In particular, the TKE equation does not contain the coriolis parameter but does contain the buoyancy effect; (8) does not contain the latter except in self-cancelling form. Hence, there are good reasons for questioning the general validity of the R_v=const assumption which led to (8).

In the present study we therefore examine assumption (7) by means of direct measurements of Δv and other relevant quantities, and attempt to fit measured values of w_e/u_* by an entrainment relation which is qualitatively consistent with the TKE equation.

2. Experimental apparatus and procedures

Our primary annulus has inner and outer diameters of 0.82 and 1.18m, respectively, giving a gap Δr of 0.183m. It is about 0.8 of the size of the one KP and KPA used, and 1.7 the size of the one used by Kantha (1978). A second, inner annulus was also occasionally utilized; its outer wall is the same structure as the inner wall of the primary annulus, and its gap is Δr = 0.099m. The walls are very smooth and their separation constant to within $\pm$ 2mm. A photograph of the apparatus is shown in Fig. 1. The annulus is situated within a penetrative convection tank

previously used in free convection studies. The rotating screen is located at the bottom of the annulus, rather than the top, because it was planned to add an upward directed heat flux through the screen in later studies. The rigid screen is flat and true to ±0.7mm, with a diamond-shaped mesh of size 6mm by 21mm. Underneath the screen are flat insulating sheets of 10mm thickness. A 5mm space between the screen and this surface is taken into account when calculating the salt-water mass budget of the lower layer; otherwise the screen is considered the z=0 level.

Two large plastic windows in the outer annulus wall permit illumination and visual observations from the side. The windows join the fiberglass sidewalls smoothly with no abutments to the flow. A horizontally spread laser beam could be positioned close to the outer edge of the mixed layer (at $z \equiv h_L$) midway between annulus sidewalls, to determine mixed-layer heights as in Deardorff et al. (1980). The mixed layer was usually made visible by adding trace amounts of non-fat milk to the lower layer. The height of the laser beam was continuously fed into a 16-channel analog-to-digital data system and stored on tape along with other signals. By comparison with some salinity profiles, it was determined (see Section 4) that $h_L \cong h_2 \lesssim 1.25h$, where h_2 is the greatest depth to which any mixed-layer fluid has penetrated at any given time. However, in experiments using temperatur h_L lay somewhat below h_2. The laser beam could also be utilized to determine the mean slope of the entrainment interface, associated with the centrifugal force. However, h_2-h could not be reliably estimated by visual methods.

Numerous plyolite particles (0.1 to 0.5mm diameter) with specific gravity of about 1.02 were also added to the water so that their passage between markers 0.2m apart could be noted and entered into the data system for conversion to mixed-layer velocities (see Fig. 1; the vertical lines are located on both side walls of the primary annulus so that parallax error is avoided). For this purpose only the central portion between side walls of the primary annulus was illuminated.

In a few experiments 0.1 mm particles were also inserted into the non-turbulent layer so that the mean flow, if any, at and beyond the outermost edge of the mixed layer could be similarly estimated. Due to momentum transfer by molecular viscosity, $v(h_2)$ turned out to be an appreciable fraction of $\bar{v}$ when w_e was small,

so that a correction had to be applied to derive Δv from $\bar{v}$ (see Section 3).

In 3 experiments particle trajectories could not always be viewed, as when using the inner annulus. A slightly heavy float of height h_f=9.7 cm was then tracked within the turbulent layer to provide $\bar{v}$. The float was equipped with a horizontal ring of diameter $0.9\,\Delta r$ which caused it to drift midway between side walls. Its velocity relative to $\bar{v}$ was calibrated in the primary annulus as a function of h_2/h_f, yielding downward corrections of 10-20% in $\bar{v}$.

In 2 SOL experiments, from which 8 entrainment data points were derived, a temperature gradient in water provided the density contrast, and the outer layer was given a linear stratification of about 1 C/cm. In 15 experiments (see Table 1) supplying 64 data points, the 2LS was employed with salt (NaCl) in the lower layer of water, and fresh or nearly fresh water in the upper layer. It may be noted that this configuration differed from that of KPA in that their fresh-water layer was the turbulent layer. However, the difference is not expected to affect the results. In one 2LS experiment of 3 data points, kaolin (clay) was used.

The friction velocity, u_*, was not measured directly but was inferred from the momentum balance or screen drag coefficient, as described in the next section.

In the 2 experiments with temperature as the stratification variable, it was measured by 2 vertically traversing thermocouples positioned midway between annulus side walls and separated 90° in arc. They were mounted from rods 3.2mm in diameter which descended into the water from above. The thermocouple heights and temperature signals were monitored continuously, with their outputs being averaged together to provide a better measure of the mean.

In the experiments using salt or kaolin, the density of the two layers was determined gravimetrically from samples withdrawn at the beginning and end of each experiment. The relative density difference, $|\Delta\rho|/\rho_o$, was kept below 6%, where ρ_o is the density of fresh water.

In 2 experiments with salt, profiles of ρ were obtained from an impedance probe (the support is visible in Fig. 1) of physical construction similar to the one

designed by Kantha (1978). One needle-like electrode is "platinized" platinum; a horizontal section of the stainless steel probe body provides the other electrode situated at the same mean height. The input ac voltage is of frequency 5 KHz; the output dc voltage is nearly linear with density for $1.004 < \rho < 1.06$ when NaCl is the constituent salt. Further details will be presented elsewhere. This probe was also traversed vertically, with density signal and height fed continuously into the data system.

For filling purposes, the annuli and surrounding tank were placed in free liquid contact by removal of a cover plate from a vertical slot in each of the walls of the two annuli. They were then partially filled with salt water of constant density to a depth of 0.05 to 0.1m; later fresh or nearly fresh water was carefully fed in from above using a floating pipe with many horizontally pointing orifices. The total water depth was 0.30m. After replacement of the wall-slot cover plates, the water in the two annuli was no longer in communication except for a 6mm gap at the bottom of the lower layer -- 5mm below the screen and 1mm above (the same screen was at the bottom of both annuli). There were also three small gaps at the bottom of the inner annulus inner wall where drive wheels in the central region (see Fig. 1) propelled the screen. The gaps were partially sealed with weatherstripping, but still allowed some diffusion of water between the primary and inner annuli, and between the inner annulus and central region. In order that this transfer not affect the salt mass budgets, in 6 of the 18 primary-annulus experiments the lower layers of the inner annulus and central region were periodically stirred as necessary so that their values of h would approximately equal h of the primary annulus. Otherwise, h grew more slowly in the inner annulus than in the primary annulus. During another 5 of the experiments a smooth plexiglass plate was attached to the upper side of the screen in the primary annulus, but not in the inner annulus. Then only the central region was mechanically stirred, the mixed-layer growth rates in the two annuli being more nearly equal. In the results to be

presented, no significant difference in scaled entrainment rates could be detected between the 11 experiments in which these precautions were taken and the 7 earlier ones in which they were not. It is concluded that the rate of diffusion of denser water from inner to outer annulus through the gap at the bottom was too slow to affect w_e. Its effect on R_τ and R_v, when detectable, was however taken into account.

Except in the 2 SOL experiments with heat, several (2-5) constant values of screen speed were employed in a series of smoothly connected steps in each experiment. In about half these cases the steps progressed upwards with time, and in the others, downwards. The length of each plateau of constant screen speed varied from 120 to 1000s, depending upon the entrainment rate, and an interval of 100s was allowed between plateaus for each new equilibrium to be achieved.

In the SOL experiments, the screen speed, v_s, was usually increased according to $v_s \propto t^{\frac{1}{2}}$, which yielded approximately constant u_* values; occasionally it was held constant, which yielded slowly decreasing u_* values (see KP). Screen rotation rate was also continuously logged into the data system, as was time after initiation of each experiment.

Prior to the start of each 2LS experiment the screen was rotated for a short period, thereby sharpening the interface. The mixed-layer velocity was then permitted to die out before actual measurements commenced. Even with this procedure, however, in some of our experiments in which the first plateau employed a small screen speed, results had to be discarded because of a much greater apparent entrainment rate during the first part of the first plateau than during the remaining part. In these instances the initial interface had apparently been left in a somewhat diffuse condition, so that the newly developing boundary layer at first deepened anomalously rapidly until the full density jump was encountered.

Temperature stratification was used in only a few of the experiments because the relatively rapid molecular diffusivity of heat in water precluded our studying the 2LS or achieving very large R_τ values. The larger R_τ values were of interest

to us when it became apparent that the centrifugal force was causing a substantial mean interfacial slope, and that only by increasing R_v and R_τ could we minimize this slope.

3. Analysis

The experimental data logged onto magnetic tape was computer processed and, in most instances, automatically plotted as in Fig. 2. In this experiment (No. 10; see Table 1) the screen speed, v_s, was initially increased to a relatively large value, then decreased in steps.

Sidewall drag. At the ends of most experiments, and as in Fig. 2, v_s was increased until $\bar{v}$ was relatively large; then v_s was decreased nearly continuously so that in the primary annulus it would match $\bar{v}$ there as closely as possible. It was found that close matching in situ could be attained through constant visual comparison of the motion of the particles in the bulk of the mixed layer relative to that of the underlying screen, as in Fig. 2 for $t > 2450$s. Then u_* was essentially zero, and it was also noted that $\partial h/\partial t$ quickly vanished after v_s was rapidly reduced. Thus, the sidewall drag coefficient, C_{DW}, could be obtained from (3), using the integrated form

$$C_{DW} = \frac{\Delta r \ (\bar{v}_1 - \bar{v}_2)}{2 \bar{v}_1 \bar{v}_2 (t_2 - t_1)} \tag{9}$$

where subscripts 1 and 2 refer to the beginning and end of the period over which $v_s = \bar{v}$.

The average value obtained from 15 such determinations is

$$C_{DW} = (3.7 \pm 0.4) \times 10^{-3} \ . \tag{10}$$

This value agrees well with the formula for turbulent flow between smooth walls adopted by Price (1979):

$$C_{DW} = 0.04 \ (\bar{v} \Delta r / \nu)^{-1/4} \tag{11}$$

where ν is the kinematic viscosity. For $\bar{v}$ = 0.075 ms^{-1}, a mean value during the u_*=0 tests, for ν = 1.0 mm^2s^{-1}, and for the constant in (11) extended to 0.040, (11) also yields 3.7×10^{-3}.

It is assumed that during entrainment the sidewall drag coefficient is still given by (11) even though stronger turbulence associated with the screen motion and with Δv is then superimposed upon the turbulence associated with lateral shear at and near the side walls. A reason for not accepting (11) without first a direct check was the possibility that sidewall curvature should alter the formula. The boundary layer at the outer concave wall is expected to be more turbulent than at the convex wall, since a laminar boundary layer at least would be expected to be unstable to Taylor-Görtler vortices at the concave wall. However, the most noticeable effect from visual observations was a reduction of turbulence near the inner wall, as noted by Kantha (1978) but not involving as extensive a region as reported for his smaller annulus.

Determination of u_*. With C_{DW} obtained from (11), (3) was preliminarily solved for u_*^2 using the experimental observations of $h_L(t)$ and $\bar{v}(t)$. As discussed earlier, h was taken to be 0.8 of the height, h_L, determined by positioning the laser beam near the outermost edge of the turbulent layer. Usually, the sidewall drag term was the dominant contributor to u_*^2. After evaluation of these data, the screen drag coefficient

$$C_{DS} \equiv u_*^2/(v_s-\bar{v})^2 \qquad (12a)$$

was calculated. Results for the primary annulus are shown in Fig. 3 as a function of the Reynolds number for the mixed layer, $h\bar{v}/\nu$. When the screen was not covered by the smooth plate (see Section 2), C_{DS} averaged

$$C_{DS} = 6.0 \times 10^{-3} \quad \text{(rough screen)}; \qquad (12b)$$

when it was covered by the plate it averaged

$$C_{DS} = 3.5 \times 10^{-3} \quad \text{(rotating smooth plate)} \qquad (12c)$$

The value in (12c) is in close agreement with (11) for $h \rightarrow 4r$, as indicated by the solid curve in the figure and the circle data points, although the scatter leaves it uncertain if the expected Reynolds number dependence was present. Because of this scatter, we utilized the values in (12b) and (12c) for C_{DS}, and calculated u_*^2 from (12a) rather than from (3) and (11) for purposes of evaluating w_e/u_* and R_τ. Examination of the data in final form, using u_* values derived from both methods, indicated less scatter when (12) was the method utilized, though either method yielded the same general results.

Our values of u_* ranged between 0.3 and 1.7 cm s^{-1} (see Table 1). Their relative uncertainty, based upon uncertainty in (12a) of 3% for v_s and 5% for ∇, is 6%. An absolute uncertainty in the mean of some $\pm$ 7% is also present, judging from the scatter of Fig. 3 and including uncertainty in the C_{DS} calculation caused by uncertainty in relating h_L to h. The net uncertainty in u_* is therefore estimated to be $\pm$ 9%.

Entrainment rate. w_e was evaluated graphically from enlarged versions of figures like Fig. 2, taking advantage of the fact that w_e was essentially constant, for the 2LS, for a constant screen speed. It was assumed that $\partial h/\partial t = 0.8 \partial h_L/\partial t$. Typically, 20-50 independent measurements of local h_L values entered into each estimate of w_e. The error in w_e due to sampling is estimated to have been $\pm$ 15%, and not less than $\pm 2 \times 10^{-4}$ cm s^{-1}.

Mixed-layer velocities. Numerous measurements of individual particle mean speeds, as in Fig. 2, were graphically averaged over each entrainment period to obtain the $\bar{v}$ values. The scatter of estimates mostly reflects sampling error rather than uncertainty in individual particle speeds. Most of the particles tracked remained in the central half, vertically, of the mixed layer during their timing, but some ranged closer to the screen or closer to z=h. The scatter provides a lower limit to an overall longitudinal turbulence intensity. For cases involving kaolin or the inner annulus, tbe buoy motion provided $\bar{v}$.

Buoyancy jump. For the 2LS, the quantity $b = g|\Delta\rho|/\rho_o$ was evaluated by asuming that $b(\bar{h}+\delta)$ varied smoothly between initial and final measured values, where $\bar{h} = \frac{1}{2}(h+h_2) \cong (9/8)h$ is a mean boundary-layer depth and $\delta \approx 8$mm is the equivalent salt-water depth below and within the screen. In many of the experiments this quantity was essentially constant, as expected for the 2LS. However, in the rough-screen experiments in which appropriate mechanical stirring in the inner annulus and central region was not provided (see Section 2), $b(\bar{h}+\delta)$ for the primary annulus increased by up to 20% during the course of an experiment. We estimate that the relative uncertainty in our measurements of $b\bar{h}$ is $\pm$5%, with a greater uncertainty, crudely set at $\pm$10%, attached to incomplete vertical mixing within the mixed layer. The same method of estimating b was employed whether or not the turbulent layer was well mixed in salinity.

For the experiments using heat, $b = g\alpha\Delta T$, where α is the coefficient of thermal expansion of the water, and ΔT is the temperature jump defined by $T(h_2)-\bar{T}$. Here, $\bar{T}$ is that mean mixed-layer temperature which at any given time yields as much warming in the inner half of the mixed layer, relative to the initial temperature profile, as there was cooling in the outer half of the mixed layer.

Velocity jump. Estimations of $v(h_2)$ described in Section 2 disclosed substantial velocities which, when scaled by $\bar{v}$, were found to correlate with the quantity $w_e(h/\nu\bar{v})^{1/2}$ as in Fig. 4. With small w_e the mixed-layer momentum has greater time to propagate viscously beyond $z=h_2$ without being overtaken by $h_2(t)$. The relationship found for $\Delta v \equiv v(h_2)-\bar{v}$ is

$$|\Delta v|/\bar{v} = 0.89 + 0.057 \ln\left[w_e(h/\nu\bar{v})^{\frac{1}{2}}\right] . \qquad (13)$$

It is ad hoc and cannot be expected to hold beyond the typical conditions encountered in our own and similar experiments. (See the Appendix for an analysis of how viscosity and time dependence are expected to have influenced Δv in Exps.16, 17.) Eq.(13) was utilized to obtain corrected values in all cases for which only $\bar{v}$, not Δv, was measured. Without this correction, estimates of R_v can be substanti-

ally too small in annulus experiments.

Owing to the experimental difficulty in identifying particles very close to $z=h_2$ and just outside of the mixed layer for tracking purposes, the relative error in Δv is estimated to be $\pm 10\%$, which is somewhat greater than suggested just by Fig. 4 and the estimated 5% uncertainty in $\bar{v}$.

As found by previous experimenters, the flow several centimeters or more beyond the interface was observed to be laminar in appearance; velocities were extremely weak except in prolonged experiments with especially small w_e values.

Combined uncertainties. The net estimated root-mean-square uncertainty in w_e/u_*, assuming independent error sources, is $\pm 17\%$, except for values less than 4×10^{-4} for which the uncertainty can approach $\pm 50\%$. The net uncertainty in R_T is similarly estimated to be $\pm 22\%$, and that of R_v, $\pm 25\%$.

4. Results

Temperature and density profiles. Temperature profiles from experiments 1 and 2 are shown in Figs. 5 and 6, respectively. Although the bulk of the mixed layer has a significant vertical gradient in T, the height h_2 can be clearly determined and h estimated to be some 20 to 25% smaller. Because $|\Delta\rho|/\rho_o$ was relatively small in these experiments with temperature, w_e/u_* was relatively large; this may have contributed to the imperfect vertical mixing inside of z=h.

Density profiles using the salinity probe were measured only during experiments 16 and 17, and are shown in Figs. 7 and 8. In Fig. 7 the profile for t=117s, for which w_e/u_* was quite large (.043), shows such a huge gradient of

ρ within the turbulent layer that no jump, $\Delta\rho$, is evident at all. Many of the density profiles of Kantha (1978) had this appearance. The other profiles of Fig. 7 were accompanied by w_e/u_* values considerably less than 0.03 and exhibited a much more uniform appearance within the bulk of the turbulent layer. In Fig. 8 for experiment 17 the density profiles are very well mixed in appearance inside of z=h, and were accompanied by still smaller values of w_e/u_* (see Table 1). The temperature profiles in Fig. 5 were accompanied by w_e/u_* values in the neighborhood of 0.025and are marginal in exhibiting a well mixed appearance. It might therefore be inferred that the extent of mixing, perhaps as measured by $h\overline{(\partial\rho/\partial z)}/\Delta\rho$, is a function of w_e/u_* (see also André et al., 1979), where $\overline{\partial\rho/\partial z}$ is the mean density gradient within the inner 3/4 or so of the turbulent layer. Also, w_e/u_*=0.03 may be a kind of threshold above which the mixing is highly incomplete. This approximate value also tends to separate Kantha's poorly mixed salinity profiles from the better mixed cases. However, due to the existence of the second velocity scale, Δv, which need not depend linearly on the first scale, u_*, this inference is uncertain.

The mean mixed-layer heights noted by the laser (near h_2) at the average time of each temperature or density profile are also denoted in Figs. 5-8.

Although no velocity profile measurements were attempted, the visual appearance of the numerous tiny particles within the turbulent layer was always one of qualitative well mixedness for all values of entrainment rate.

Interfacial slopes. During several of the experiments h_2 was measured near the inner and outer sidewalls of the primary annulus, and the associated slope over a distance of 0.15m determined. From the balance of forces for the lateral velocity component the expected slope is

$$s = \bar{v}^2/(g\bar{r}\,|\Delta\rho|/\rho_o) \qquad (14)$$

where $\bar{r}$ is the mean radius. A scatter diagram of individually measured slopes

versus expression (14) is presented in Fig. 9. Although the data for small interfacial slopes lie close to the 1:1 line, the observed slopes are unexplainably smaller than the theoretical ones for values of the latter exceeding 0.10 to 0.15. However, slopes exceeding even 0.1 or 0.2 are relatively large in the present context, and are undesirable at least for the reason that entrainment must be occurring horizontally (u_e) as well as vertically (w_e). Only the vertical component is of direct interest here.

Overall, the net entrainment, $\underset{\sim}{V}_e$, is always considered to act normal and outward to the mean plane of the turbulent fluid interface, as in Fig. 10. Only if $\partial h/\partial r$ is small will u_e/w_e be correspondingly small. Considering that other uncertainties in w_e/u_* discussed in Section 3 lie around $\pm$17%, we regard the uncertainty caused by horizontal entrainment ($u_e \approx 0.1$ to $0.2 w_e$) to be of comparable magnitude and not cause for rejection of the data. It may be pointed out that horizontal entrainment does not occur freely despite the lack of a gravitational restoring force; there is a corresponding restoring force, from the viewpoint of parcel stability, associated with either the lateral pressure gradient or the centrifugal force (see Veronis, 1970).

It is not understood why slopes of similar magnitude were not reported by previous investigators. We expect the interfacial slope to have essentially the same magnitude whether the rotating mixed layer occupies the upper or the lower portion of a two-layer system. However, L. H. Kantha (personal communication) states that substantial slopes were observed, especially in his smaller annulus.

The failure of the observed interfacial slopes to obey (14) at larger slopes may have been associated with a strong decrease of h_2-h in proceeding from the inner to the outer annulus wall, so that $(\partial h_2/\partial r) < (\partial h/\partial r)$. Another possibility is that it was associated with a centrifugal secondary circulation which is upwards at the outer wall. This circulation was quite evident during the start-up of each experiment when an interfacial slope is becoming established, and also dur-

ing acceleration of the rotating screen at other times. However, in agreement with previous observations, it was scarcely evident during the measurements with constant, or quasi-constant, screen speed.

Entrainment versus R_τ and R_v. Our main results on entrainment are shown in Fig. 11 where w_e/u_* is plotted against R_τ, as is conventional. Also shown is the data swath from KPA. The latter lies above our data, the customary explanation being that $h/\Delta r$ is larger for our data (our values of $h/\Delta r$ range from 0.38 to 1.5 and average 0.7, while those presented by KPA were smaller than 0.5). Eq.(8) can then be invoked to show the effect of increased sidewall friction in decreasing w_e/u_*.

However, our measured values of R_v are printed at the data points of Fig. 11, and they indicate how R_v increases from values near 1 up to 5 or 10 or more, as R_τ increases from 50 to 1000. Although this is not surprising in view of the high positive correlation between Δv and u_*, it means that the R_v = const. concept which leads to (8) cannot be upheld unless almost all the data is rejected on the grounds that $h/\Delta r$ was too large. On the other hand, if $h/\Delta r$ were as small as 0.1 or 0.2, the turbulence Reynolds number proportional to hu_*/ν would be considerably less than 500. The data could be rejected as not applying to the large Reynolds-number regime in which the value of ν is irrelevant except for wall effects.

We therefore wish to introduce an alternative interpretation of the results. Suppose, as discussed in Section 1, (8) is not an entrainment law in general even for a laboratory annulus experiment. Assumption (7) then need not be considered valid in general, and conditions which cause R_v to increase beyond some expected critical value near unity need not be excluded from consideration. In particular, the laboratory entrainment results may be essentially valid even when the left-hand side of (3) is of minor importance relative to u_*^2. Then

$$R_v/R_\tau = u_*^2/(\Delta v)^2 \cong u_*^2/(\bar{v})^2 \cong 2C_{DW}h/\Delta r \qquad (15)$$

indicating that R_v will increase along with R_τ and faster when $h/\Delta r$ is greater. For any given band of R_τ values our data tend to show this relationship, there being a spread in R_v values such that greater R_v tends to be associated with greater $h/\Delta r$.

The alternative interpretation comes from noticing that, for a given narrow band of R_τ values, w_e/u_* is highly correlated, inversely, with R_v. This is to be expected (since $R_v \propto (\Delta v)^{-2}$) from consideration of the TKE equation wherein Δv is a source of TKE at the entrainment interface (see Mahrt and Lenschow, 1976; Zeman and Tennekes, 1977; Price et al., 1978) and contributes towards entrainment. Thus we prefer to consider w_e/u_* to be a function of both R_τ and R_v, and the sloping lines in Fig. 11 represent our attempt at estimating a simple functional dependence which best fits our 2LS data. This dependence is

$$w_e/u_* = 0.33 R_\tau^{-\frac{1}{2}} R_v^{-1.4} \quad . \tag{16a}$$

It should be emphasized that these sloping lines are hand-fitted estimates of the R_v values actually encountered, and are not assumptions for different critical R_v values. An alternate form of (16a) is

$$w_e/|\Delta v| = 0.33 R_\tau^{-1} R_v^{-0.9} \quad . \tag{16b}$$

In (16a), the $R_\tau^{-\frac{1}{2}}$ dependence, if R_v should happen to be constant, comes entirely from the arguments of Price (1979) and Thompson (1979), using (5) and (7), upon considering the case when no sidewall friction is present. However, we consider this dependence to remain valid even when considerable sidewall friction is present, and the inverse R_v dependence to account for the deviations from an $R_\tau^{-\frac{1}{2}}$ dependence. Eq.(5) does not yield entrainment information for the opposite case of R_τ constant and R_v variable, since $(\partial/\partial t)R_v \neq 0$ then and (5) remains a momentum-budget equation which can say nothing about the entrainment

rate.

Eq.(16a) closely resembles the entrainment relation proposed by Kantha (1978) and mentioned in Sec. 1, except that we find the R_v exponent to lie near -1.4 instead of -0.5.

Eqs.(16a,b) are based upon the use of h as length scale. If $\bar{h} \cong (9/8)h \cong (9/10)h_2$ is used instead, (16a) becomes

$$\bar{w}_e/u_* = 0.47\ (\bar{R}_\tau)^{-\frac{1}{2}}\ (\bar{R}_v)^{-1.4} \qquad (16c)$$

where the overbars here refer to the use of $\bar{h}$ in the definitions. The precise definition adopted for the boundary-layer depth thus has a substantial influence (40% in this instance) on the proportionality constant.

If sidewall friction were to become so large that associated lateral velocity

gradients near the side walls were an important factor, along with Δv and u_*, in generating and maintaining mixed-layer turbulence, then we should expect w_e/u_* to depend also upon a sidewall friction velocity. w_e/u_* would then be enhanced, rather than damped, for given values of R_τ and R_v. Also, if $h/\Delta r$ much exceeds unity we might expect deviations from a dependence of w_e/u_* upon only R_τ and R_v because of insufficient space for lateral eddy scales. However, for $h/\Delta r$ as huge as 1.5 we see no dramatic evidence from Fig. 11 that these other factors were very important, considering the data uncertainties discussed in Section 3. In particular, the 5 underlined data points for the 2LS are from the inner annulus where Δr was only 0.54 as large as for the primary annulus, and they fit in reasonably well with the rest of the data. However, there is a systematic tendency for data points at large R_τ and large R_v to have somewhat enhanced values of w_e/u_* relative to the overall fitted functional dependence. This may reflect excess turbulence energy generation due to sidewall friction when $|\Delta v|$ was too small to mask it.

Except for this tendency, the data uncertainties discussed in Section 3 appear capable of explaining the scatter of the 2LS data points relative to (16a). (The uncertainty in u_* spreads the data points in a direction normal to the R_v = constant lines in Fig. 11.) Because of the scatter, the exponent of R_v in (16) is not yet well determined, nor is the second decimal place of the proportionality constant accurately known. The SOL data in Fig. 11 will be discussed in Section 5; the 3 kaolin 2LS data points fit in well with the salt data.

5. Comparison with other experiments

SOL vs 2LS experiments. With the portrayal of w_e/u_* of Fig. 11 we no longer expect any distinction in entrainment between the SOL and 2LS experiments (KP vs KPA) that is not accounted for by a distinction in R_v. In the SOL experiment R_τ starts out very small and progresses rapidly to larger values, since

$bh = (g/\rho_o)\,|\partial\rho/\partial z|_{outer} h^2/2$ increases as $h^2(t)$. In the 2LS experiment with u_* constant, R_τ is constant; R_v starts out extremely large because of the finite initial h and requires on the order of 100s (or u_*t/h = 10 or 20) before it reaches a quasi-constant minimum value (Price, 1979, Fig. 3). When the assumption R_v=const. is not made, it is not clear if, in comparing the two types of initial-value experiments at the same R_τ, that the 2LS experiment obeying (16) will have a smaller R_v value and consequently greater entrainment than the SOL experiment, as in KPA versus KP.

To check this point, a time dependent numerical model was constructed obeying (16c), (11), (13) and (3), with the left-hand side of the latter modified to yield an entrainment momentum flux of $-\Delta v\, w_e$ instead of $\bar{v}w_e$. The model was utilized on the KP case with initial conditions: $\bar{h}(0)$=0.5cm, $(1/\rho_o)\,|\partial\rho/\partial z|_{outer}$ = 7.67 x 10^{-3}cm^{-1}, and with $\Delta\rho/\rho_o = \frac{1}{2}(\bar{h}/\rho_o)(\partial\rho/\partial z)_{outer}$; and on 5 KPA cases with initial conditions: $\bar{h}(0)$=5.4 cm and initial $\Delta\rho/\rho_o$ values yielding R_τ = 36.2, 70.3, 150.4, 292 and 523. In all cases u_* was 1.41 cm s^{-1}, Δr was 22.8 cm and $\bar{v}(0)$=0. Results are those of Fig. 12, the 2LS data points being those occurring when R_v had dipped to its minimum value and was most steady, for which $\bar{h}/\Delta r$ was in the vicinity of 0.4. The functional dependence of (16) is seen from Fig. 12 to have reproduced, qualitatively, the difference observed between the KP and KPA experiments; the latter are predicted to entrain at a rate about 1.7 times greater. However, the KP experiment is overpredicted at the larger R_τ values.

The explanation for the smaller R_v values, and consequently greater w_e/u_* values enjoyed by the 2LS, is threefold and no longer as simple as when R_v is assumed constant. At an early stage, the explanation comes from noting that the normalized time (u_*t/h) at which $(R_\tau)_{SOL}$ reaches $(R_\tau)_{2LS}$ is less than the time at which $(R_v)_{2LS}$ has dipped to its minimum value. At this stage, when

sidewall friction may be ignored, and assuming $-\Delta v = \bar{v}$, (3) integrates to

$$\bar{v}/u_* = u_* t/h \quad . \tag{17}$$

Thus $\bar{v}/u_*$ was greater for the 2LS, at the same R_τ, because mixed-layer acceleration occurred over a longer time period for the 2LS. It follows from definitions (2) and (4) that $(R_v)_{2LS} < (R_v)_{SOL}$ and hence, from (16a), that $(w_e)_{2LS} > (w_e)_{SOL}$. In the cases treated by Fig. 12, $(\bar{R}_\tau)_{SOL}$ reached 36.2, 70.3 and 150.7 when $(u_* t/\bar{h})_{SOL}$ was 6.7, 9.9 and 15.5, respectively. The corresponding dimensionless times at which $(\bar{R}_v)_{2LS}$ was most steady were greater: 8.0, 11.8, and 19.0. The ratio between the mixed-layer velocities in the two cases becomes nearly cubed, through (4) and (16c), in its effect upon the entrainment ratio.

At a later stage, controlled by wall friction, $(\bar{v}/u_*)_{2LS} > (\bar{v}/u_*)_{SOL}$ when $(R_\tau)_{SOL} = (R_\tau)_{2LS}$ because $(h/\Delta r)_{SOL}$ had become appreciably larger than $(h/\Delta r)_{2LS}$. Sidewall friction was then stronger for the SOL case. When $(\bar{R}_\tau)_{SOL} = 292$ in Fig. 12 and $(\bar{R}_v)_{2LS}$ had reached its broad minimum value, $\bar{h}_{SOL}$ was 12.5cm while $\bar{h}_{2LS}$ was only 7.7 cm. This occurred for $(u_* t/\bar{h})_{SOL}$=27.1 and $(u_* t/\bar{h})_{2LS}$=29.3. This second explanation takes over well before the first one no longer holds.

In both cases, since $(w_e)_{2LS} > (w_e)_{SOL}$, $|\Delta v|/\bar{v}$ is closer to unity for the 2LS because of the viscous effect, parameterized by (13). This effect enhances $(R_v)_{SOL}/(R_v)_{2LS}$ and amplifies somewhat the entrainment rate advantage of the 2LS in the laboratory.

With representation (16) there is thus no particular relevance to a finding of greater w_e/u_* for the 2LS than for the SOL, unless both R_τ and R_v are matched in the two cases.

Salt versus temperature. Bearing the preceeding discussion in mind, the temperature data points in Fig. 11 lie anomalously above the salt points, considering their larger R_v values. If, for R_τ near 100 the temperature data obeyed (16a), their w_e/u_* values would be roughly a factor of two smaller than observed.

However, similar behavior was observed in the oscillating-grid entrainment experiments of Turner (1968) and of Wolanski and Brush (1975). In those experiments an oscillating-grid velocity scale replaces u_*, and R_v is infinite and irrelevant. The entrainment differential became small or vanished as their equivalent R_τ variable became small. Wolanski and Brush looked for a turbulence Reynolds number dependence, but found none. According to Crapper and Linden (1974) this may have been a Peclet number (Pe) effect, with Pe being sufficiently large when using salt that its value was immaterial, but not when using heat. Here, Pe will be defined by hu_*/D, where D is the (molecular) kinematic diffusivity in water. Our experiment with kaolin supports this conclusion, since the Brownian-motion value of D for kaolin (with particle diameters observed to be near 1μm) is several orders of magnitude smaller than D for salt. In preparing the kaolin suspension a small amount (0.5%) of a deflocculating agent was added in order to minimize problems with the kaolin settling out. This agent was comprised of equal parts by weight of sodium silicate solution and soda ash. However, even if this agent had a molecular diffusivity of magnitude near that of salt, its molecular diffusion across the local entrainment interface could have had no conceivable effect upon the net density contrast. In contradiction, Wolanski & Brush did obtain very significant further decreases in entrainment rate upon utilizing fluid suspensions, one of these also being kaolin. McDougall (1979) has conjectured that this result may have been some effect of a non-Newtonian viscosity of the suspension. However, we investigated the viscosity of our kaolin suspension, using a falling-sphere viscometer, and found only the expected gradual monotonic increase of apparent viscosity as the density of the suspension increased from 1.00 to 1.05. The results of Wolanski & Brush on suspensions therefore remain unexplained in our opinion.

The present results thus suggest the possibility that the molecular diffusion coefficient somehow causes enhanced entrainment for R_τ values exceeding about 50

(or R_v exceeding about 1.3) when Pe is of order 10,000 or less, and not when Pe is 100 or more times greater.

Single velocity-scale experiments. Entrainment relation (16b) may prove useful in helping interpret entrainment experiments designed to have only one velocity scale, Δv. If the present 2LS data are plotted as $w_e/|\Delta v|$ versus R_v and the u_* velocity scale is ignored, they appear as in Fig. 13. The inner-annulus data with larger R_v values, which were associated with large $h/\Delta r$ values, now appear anomalous. In those cases, $u_*/|\Delta v|$ was substantially larger for the inner annulus, indicating the need for the u_* velocity scale in addition to $|\Delta v|$.

In the pioneering experiment of Ellison & Turner (1959) a layer of (turbulent) fresh water flowed over a weir and then over a stagnant saline solution (along x), the two layers having a velocity differential Δv. However, there was a second velocity scale in the upper layer associated with that entire layer remaining turbulent after flowing over the weir while the saline layer was non-turbulent. This velocity scale was neglected. Since, moreover, it was x-dependent and not associated with surface shear, results of their experiment can scarcely be compared with those of annulus experiments. Nevertheless, the lower range of their data is shown in Fig. 13 to indicate that theirs was a small-R_v experiment.

The experiment of Lofquist (1960) comes close to being a rectilinear version of the annulus experiment. A layer of salty water was caused to flow under a stagnant, neutral fresh-water layer, and the entrainment rate of the former into the latter was deduced and interpreted, again only using the Δv velocity scale. The second unused velocity scale was probably associated mainly with bottom and sidewall friction. His mean data curve is shown in Fig. 13. It lies close to the present data, which is not surprising since his flow velocities were of comparable magnitude (2 - 13 cm s^{-1}) and similar u_* values must have occurred.

The small value of the proportionality constant, c, incurred in such an experiment when analyzed as $w_e/|\Delta v| = cR_v^{-n}$ can therefore be explained by $n \cong -0.9$ and c representing $0.3R_\tau^{-1}$ as in (16b), with R_τ ranging between 200 and 1200.

In the experiment of Moore and Long (1971) jets with compensating suction at the bottom and top plates of a toroid propelled two turbulent layers of contrasting density in opposite directions. Their mean data curve is also shown in Fig. 13 after adjusting R_v to contain the length scale h. It is not clear whether the most important second velocity scale here was associated with the jets emitted from the slots in the bottom and top surfaces, or with bottom friction and/or sidewall friction. If the appropriate second velocity scale is taken to be proportional to Δv, one would expect from (16b) an approximate $R_v^{-1.9}$ dependence for their data in Fig. 13. The much less steep observed dependence, and the smaller dimensionless entrainment at the smaller R_v values, may have been caused by presence of a central laminar region for $R_v < 3$ or 6 (see their Fig. 4 and discussion on p.644). The scaling quantities $|\Delta v|$ and $|\Delta \rho|$ then each become a factor of 2 or more smaller which would displace the curve upwards and to the right. This interpretation presupposes that the appropriate values of Δv and $\Delta \rho$ represent property differences between well-mixed values and non-turbulent outer-edge values.

6. Summary of results

It is found that in annulus mixed-layer experiments where turbulence and entrainment are driven by a rotating screen, u_* can be determined satisfactorily from the momentum budget provided mixed-layer velocities are measured. A check of this conclusion came from replacing the rough screen with a smooth surface and finding that the calculated screen drag coefficient was reduced to the value appropriate for a smooth plate. Another check is that the entrainment relation from the present study can satisfactorily reproduce the result of the KP and

KPA studies.

The entrainment interface is found to slope outwards with radius, with a slope as large as 0.1 to 0.2 when treating the smaller R_v values within our annulus. Large slopes are undesirable because horizontal entrainment is then a substantial fraction of vertical entrainment.

Judging from temperature and density profiles, the turbulent layer is found to be quite well mixed in appearance provided w_e/u_* does not exceed about 0.03 (or $w_e/|\Delta v|$ does not exceed about 0.003). The thickness of the transition layer across which the density changes, in the mean, from the well-mixed value to the outer-layer value is found to be some 25% of the well-mixed depth, h.

The inverse Froude number, R_v, is found to vary substantially in the experiments. Only in the 2LS experiment does it dip to a quasi-constant minimum value before rising, but the minimum value reached tends to increase with increasing R_τ in different experiments.

A functional dependence of scaled entrainment on both R_τ and R_v is obtained in (16a): $w_e/u_* = 0.33 R_\tau^{-\frac{1}{2}} R_v^{-1.4}$. The $R_\tau^{-\frac{1}{2}}$ dependence comes from the studies of Price (1979) and Thompson (1979), using the additional argument that no explicit dependence on wall friction should occur unless such friction generates appreciable turbulence kinetic energy. The $R_v^{-1.4}$ dependence comes from the present 2LS data. Together, the dependence indicates that both u_* and Δv promote w_e, with the Δv effect being the stronger.

With this representation the relatively smaller entrainment rate in the KP (SOL) experiment than in the KPA (2LS) experiment is found in early stages to be related to the smaller dimensionless time for the SOL case at which results are compared in the two types of experiments. In later stages it is found to be due to greater relative mixed-layer depths then occurring in the SOL case which increases R_v through sidewall damping of $\bar{v}$.

Direct observational estimates of $|\Delta v|$ disclose that it is typically significantly smaller than $\bar{v}$ due to viscous transfer of momentum into the non-turbulent outer layer. The effect is greatest when w_e is least. The present data were corrected for this effect, which causes R_v to be substantially greater than otherwise suspected.

The cases studied using temperature (large D) instead of salt to provide the interfacial density jump suggest enhanced entrainment, relative to that predicted by (16). This result might be the same phenomenon observed by Turner (1968) and Wolanski and Brush (1975) in oscillating grid experiments. An experiment utilizing kaolin (small D) to provide the density contrast in the 2LS indicated no significant difference in scaled entrainment from the experiments utilizing salt.

Comparison of the present 2LS data with other entrainment experiments designed to have only one velocity scale, Δv, indicates strong similarity when $w_e/|\Delta v|$ is plotted against R_v. This result suggests that the second velocity scale in those experiments associated with maintaining one or both of the layers turbulent was also important, as was u_* in the present experiments.

Although the present study made use of a wide range of $h/\Delta r$ values in order to achieve variable sidewall friction and a consequently wide range of R_v values, in all other respects small values of $h/\Delta r$ are desirable, along with small values of $\Delta r/\bar{r}$ and very small values of $h/\bar{r}$.

Acknowledgments. This study was supported by the Office of Naval Research, and in part by the National Science Foundation, Division of Atmospheric Sciences, under grant ATM 77-24507. The technical expertise of P. Stockton in all phases of the experimental work and data collection was indispensable. Helpful suggestions for improving the experiments were made by P. Katen, and his assistance during experiments, along with that of S. Yoon, is greatly appreciated; much laborious plotting was avoided thanks to graphical displays they provided using the plotting device kindly loaned by the O.S.U. Air Resources Center. Helpful comments on the manuscript by L. Mahrt, L. Kantha, O. Zeman and J. C. André are greatly appreciated.

Appendix. Viscous propagation of momentum beyond the interface.

In order to explore the plausibility of the results of Fig. 4 and parameterization (13), the Navier-Stokes equation was solved numerically in the region $h \lesssim z \lesssim H$, where H is the total water depth. The coordinate system was moved vertically at the speed w_e whereupon the tangential momentum equation, averaged laterally (radially), becomes

$$\partial \bar{v}_c/\partial t = w_e \partial \bar{v}_c/\partial z - (\partial/\partial z)\overline{v'w'} + \nu \partial^2 \bar{v}_c/\partial z^2 - 2C_{DW}\bar{v}_c^{\,2}/\Delta r \qquad \text{(A1)}$$

where $\bar{v}_c$ is the velocity component relative to the moving coordinate system based at z=h. The height h_2 was assumed given by 1.25h, and $(\partial/\partial z)\overline{v'w'}$ by

$$(\partial/\partial z)\overline{v'w'} = (u_*^2/h + w_e \Delta v/h)(-5 + 4z/h) \qquad (h \lesssim z \lesssim h_2) \qquad \text{(A2)}$$

$$(\partial/\partial z)\overline{v'w'} = 0 \qquad (z > h_2) \qquad \text{(A3)}$$

where $\Delta v = \bar{v}_c(h_2) - \bar{v}_c(h)$.
(A2) interpolates the turbulent frictional force linearly between its known value at the top of an ideally mixed layer and zero value at h_2.

The wall-drag term (last term) in (A1) was calculated both using the turbulent expression for C_{DW} of (11) and the laminar expression appropriate for a parabolic lateral profile, the larger of the two drag forces being used.

At z=h(t), $\bar{v}_c$ was taken to be 0.9 of the well-mixed speed, $\bar{v}$; at z=H it was assumed that $\partial \bar{v}_c/\partial z = 0$. Observed initial heights were used for h(0), along with the observed values of w_e, $\bar{v}$ and u_* as step functions of time from Exps. 16 and 17. The leapfrog numerical scheme was employed, with the damping terms lagged one time step (Δt = 2 to 5s) and with a vertical increment of 0.5 cm. The two numerical integrations were continued over the lifetime of the two experiments (see Table 1).

Results are shown in Fig. A1 where $|\Delta v|/\bar{v}$ is plotted versus $w_e(h/\nu\bar{v})^{\frac{1}{2}}$ on the abscissa. The results suggest that molecular viscosity was responsible for

a time-dependent upper limit to $|\Delta v|/\bar{v}$ that can be significantly less than unity. However, comparison with (13) suggests that this upper limit was only reached during those portions of experiments having small values of u_*, $|\Delta v|$ and w_e. Some mechanism other than molecular viscosity may therefore have been important at other times. This mechanism may have been wave momentum transport associated with external gravity waves centered near $z=h_2$, and/or internal gravity waves in the SOL experiments. The wave amplitudes must increase with increased values of $|\Delta v|$ and u_*. The numerical results thus do lend some plausibility to (13). Although the abscissa stands in need of modification that would include gravity-wave effects, (13) is used here in estimating Δv in the annulus, when $v(h_2)$ was not measured, because of the good data-point correlation of Fig. 4.

TABLE 1. Experimental data. Values represent averages over the indicated time period. No comments in last column refer to the 2LS using salt in the primary annulus above the rough screen, with Δv obtained from $\bar{v}$ using Eq.(13). Comments: [1] the SOL using temperature; [2] inner annulus; [3] smooth plate on top of screen in primary annulus only; [4] Δv obtained from direct velocity measurements on both sides of interface; [5] the 2LS using kaolin.

Exp. No.	Time (s) Begin	End	v_s (cm s^{-1})	$\bar{v}$ (cm s^{-1})	$\frac{\lvert\Delta\rho\rvert}{\rho_o}$	h (cm)	u_* (cm s^{-1})	$\lvert\Delta v\rvert$ (cm s^{-1})	R_τ	R_v	$\frac{w_e}{u_*}$	Comments
1a	200	400	11.3	4.8	0.0019	14.6	0.50	3.8	109	1.9	0.030	[1]
b	400	600	11.3	5.2	0.0023	16.4	0.47	3.9	167	2.4	0.016	[1]
c	800	950	13.5	6.4	0.0028	20.8	0.55	5.0	189	2.3	0.024	[1]
2a	150	250	9.0	2.4	0.0006	8.8	0.51	2.0	20	1.3	0.066	[1]
b	250	400	11.4	3.8	0.0013	12.4	0.59	3.1	45	1.6	0.043	[1]
c	400	550	11.8	4.8	0.0017	15.1	0.54	3.7	86	1.8	0.019	[1]
d	550	725	12.5	5.5	0.0020	17.2	0.54	4.4	116	1.7	0.027	[1]
e	725	920	13.8	6.0	0.0023	19.7	0.60	4.7	123	2.0	0.021	[1]
3a	300	700	19.2	11.3	0.036	8.8	0.61	6.6	834	7.1	0.0013	
b	700	1150	19.3	11.8	0.035	9.0	0.58	6.4	918	7.5	0.0006	
4a	600	1100	19.9	11.9	0.057	6.5	0.62	6.8	944	7.8	0.0011	
b	1200	1700	25.4	14.3	0.054	7.1	0.86	8.8	508	4.9	0.0019	
c	1800	2300	30.5	16.5	0.050	8.3	1.08	10.9	349	3.4	0.0032	
d	2400	2800	35.5	17.8	0.040	11.2	1.47	12.3	208	3.0	0.0037	
5a	100	400	35.9	19.0	0.051	8.2	1.31	13.6	239	2.2	0.0080	
b	500	900	30.4	17.3	0.036	12.2	1.01	11.6	422	3.2	0.0034	
c	1000	1500	25.6	14.4	0.034	13.4	0.87	9.0	590	5.5	0.0017	
d	1600	2100	20.6	12.0	0.033	14.1	0.67	6.2	1016	12	0.0003	
6a	1000	1500	19.9	12.2	0.033	7.4	0.60	7.4	665	4.4	0.0022	
b	1600	1900	25.2	14.1	0.030	8.8	0.86	9.6	350	2.8	0.0056	
c	2000	2400	29.8	16.1	0.025	11.9	1.06	11.6	259	2.2	0.0079	
7a	100	400	35.3	16.8	0.025	10.7	1.43	12.7	128	1.6	0.012	
b	500	800	30.1	15.3	0.018	15.4	1.15	11.0	205	2.2	0.0064	
c	900	1300	25.5	12.7	0.016	17.3	0.99	8.5	277	3.8	0.0026	
d	1400	1900	20.5	10.5	0.016	18.2	0.77	6.5	481	6.8	0.0013	
8a	600	1100	20.1	11.9	0.029	7.6	0.64	7.3	527	4.1	0.0023	
b	1200	1700	24.9	13.8	0.024	9.4	0.86	9.3	299	2.6	0.0043	
c	1800	2070	29.7	15.2	0.019	12.6	1.12	11.2	187	1.9	0.0095	
d	2200	2433	34.8	16.2	0.0127	19.4	1.44	12.8	116	1.5	0.0153	
9a	100	500	10.2	6.0	0.021	6.4	0.33	3.4	1209	11	0.0015	
b	600	1000	15.3	9.4	0.017	8.2	0.46	5.7	646	4.2	0.0024	
c	1100	1400	20.0	11.9	0.015	9.2	0.63	8.0	341	2.1	0.0057	
d	1500	1730	24.7	13.1	0.0128	11.1	0.90	9.3	172	1.6	0.0074	
e	1800	2040	29.4	13.9	0.0092	15.7	1.20	10.9	98	1.2	0.0179	

TABLE 1 (Cont'd.)

Exp. No.	Time (s) Begin	End	v_s (cm s^{-1})	$\bar{v}$ (cm s^{-1})	$\frac{\lvert\Delta\rho\rvert}{\rho_*}$	h (cm)	u_* (cm s^{-1})	$\lvert\Delta v\rvert$ (cm s^{-1})	R_τ	R_v	$\frac{w_e}{u_*}$	Comments
10a	100	250	29.7	12.8	0.016	9.7	1.31	10.2	89	1.5	0.026	
b	350	550	25.0	11.8	0.011	14.7	1.02	8.9	152	2.0	0.012	
c	650	985	19.9	10.2	0.0096	16.5	0.75	6.7	276	3.5	0.0026	
d	1000	1550	15.0	8.3	0.0092	17.1	0.52	4.7	570	7.0	0.0007	
e	1700	2275	9.1	4.4	0.0090	17.4	0.36	2.4	1184	27	0.0004	
11a	350	800	15.0	9.1	0.0117	6.3	0.46	5.8	341	2.1	0.0042	
b	900	1150	20.0	10.6	0.0091	8.3	0.73	7.7	139	1.2	0.0125	
c	1250	1490	24.9	11.2	0.0051	15.5	1.06	9.1	69	0.9	0.028	
12a	100	540	25.0	15.3	0.050	6.7	0.75	9.4	584	3.7	0.0023	
b	640	1120	29.7	16.3	0.041	8.5	1.04	10.6	316	3.0	0.0028	
c	1220	1520	35.3	17.4	0.032	11.3	1.39	12.6	183	2.2	0.0067	
d	1620	1850	40.3	18.6	0.023	16.3	1.68	14.3	130	1.8	0.0106	
13a	100	195	25.0	11.9	0.0113	8.0	1.01	9.3	87	1.0	0.026	
b	260	395	20.6	11.3	0.0099	10.0	0.72	8.1	187	1.5	0.0099	
c	470	960	15.4	8.3	0.0094	11.1	0.55	5.2	338	3.8	0.0022	
d	1065	1930	10.1	5.4	0.0093	11.4	0.36	2.8	802	13	0.0004	
14a	100	200	30.0	11.4	0.0065	9.3	1.10	9.4	49	0.7	0.045	[3]
b	300	450	25.3	10.2	0.0048	14.1	0.89	7.8	84	1.1	0.014	[3]
c	600	950	20.8	8.3	0.0043	16.8	0.63	6.0	178	2.0	0.0089	[3]
d	1100	1550	15.6	6.2	0.0041	18.1	0.43	4.1	393	4.3	0.0033	[3]
e	100	200	21.1	10.3	0.0064	8.6	0.84	8.4	76	0.8	0.051	[3], [2]
f	300	450	17.8	8.0	0.0047	11.9	0.76	6.0	95	1.5	0.014	[3], [2]
g	600	950	14.7	6.4	0.0041	13.7	0.64	4.5	134	2.7	0.0061	[3], [2]
h	1100	1550	11.0	4.6	0.0038	14.8	0.50	3.0	220	6.1	0.0022	[3], [2]
15a	100	3070	15.4	8.3	0.010	7.2	0.42	5.3	400	2.5	0.0023	[3], [4]
b	3170	3680	20.3	9.6	0.0077	10.2	0.63	6.6	194	1.8	0.0065	[3], [4]
c	3780	4035	25.1	11.1	0.0059	14.3	0.83	8.1	120	1.3	0.0151	[3], [4]
d	4120	4255	30.1	11.3	0.0044	20.0	1.11	7.9	70	1.4	0.021	[3], [4]
e	100	3070	10.8	4.3	0.011	5.4	0.50	2.5	233	9.3	0.0011	[3], [2]
16a	100	150	40.0	15.3	0.0147	10.6	1.46	12.5	72	1.0	0.043	[3], [4]
b	215	265	34.6	14.6	0.0111	15.0	1.18	11.7	117	1.2	0.019	[3], [4]
c	350	430	30.0	13.1	0.0102	17.1	1.00	10.2	171	1.6	0.016	[3], [4]
d	500	830	25.3	11.1	0.0096	18.6	0.84	8.1	248	2.7	0.0040	[3], [4]
e	930	2620	20.1	8.6	0.0088	20.4	0.68	5.1	380	6.8	0.0014	[3], [4]
17a	100	1600	20.8	10.8	0.024	10.4	0.59	6.6	703	5.6	0.0015	[3], [4]
b	1740	2060	25.6	12.6	0.022	11.8	0.77	7.2	429	4.9	0.0029	[3], [4]
c	2160	2420	30.0	14.1	0.020	13.0	0.94	9.3	288	2.9	0.0043	[3], [4]
d	2520	2780	35.2	15.2	0.017	15.8	1.18	11.5	189	2.0	0.0091	[3], [4]
18a	980	1540	28.3	12.7	0.019	11.8	0.92	9.0	260	2.7	0.0066	[3], [5]
b	1650	2600	24.5	10.9	0.015	15.3	0.80	7.3	351	4.2	0.0032	[3], [5]
c	2800	5200	19.9	8.5	0.013	17.6	0.67	5.0	499	9.0	0.00074	[3], [5]

REFERENCES

André, J. C., P. Lacarrere, & Mahrt, L. J. 1979 Sur la Distribution Verticale de l'Humidité dans une Couche Limite Convective. J. Rech. Atmos., 13, 135-146.

Crapper, P. F. & Linden, P. F. 1974 The structure of turbulent density interfaces. J. Fluid Mech. 65, 45-63.

Deardorff, J. W., Willis, G. E. & Stockton, P. 1980 Laboratory studies of the entrainment zone of a convectively mixed layer. J. Fluid Mech. 100, 41-64.

Ellison, T. H. & Turner, J. S. 1959 Turbulent entrainment in stratified flows. J. Fluid Mech. 6, 423-448.

Kantha, L. H. 1978 On surface-stress-induced entrainment at a buoyancy interface. Dept. Earth Planet. Sci., Johns Hopkins Univ. Rep. GFDL TR 78-1.

Kantha, L. H., Phillips, O. M. & Azad, R. S. 1977 On turbulent entrainment at a stable density interface. J. Fluid Mech. 79, 753-768.

Kato, H. & Phillips, O. M. 1969 On the penetration of a turbulent layer into stratified fluid. J. Fluid Mech. 37, 643-655.

Lofquist, K. 1960 Flow and stress near an interface between stratified fluids. Phys. Fluids 3, 158-175.

Mahrt, L. & Lenschow, D. H. 1976 Growth dynamics of the convectively mixed layer. J. Atmos. Sci. 33, 41-51.

McDougall, T. J. 1979 Measurements of turbulence in a zero-mean-shear mixed layer. J. Fluid Mech. 94, 409-432.

Moore, M. J. & Long, R. R. 1971 An experimental investigation of turbulent stratified shearing flow. J. Fluid Mech. 49, 635-655.

Pollard, R. T., Rhines, P. B. & Thompson. R. O. R. Y. 1973 The deepening of the wind-mixed layer. Geophys. Fluid Dyn. 3, 381-404.

Price, J. F. 1979 On the scaling of stress-driven entrainment experiments. J. Fluid Mech. 90, 509-529.

Price, J. F., Mooers, C. N. K. & Van Leer, J. C. 1978 Observation and simulation of storm-driven mixed-layer deepening. J. Phys. Ocean. 8, 582-599.

Thompson, R. O. R. Y. 1979 A re-examination of the entrainment process in some laboratory flows. Dyn. Atmos. Oceans 4, 45-55.

Turner, J. S. 1968 The influence of molecular diffusivity on turbulent entrainment across a density interface. J. Fluid Mech. 33, 639-656.

Veronis, G. 1970 The analogy between rotating and stratified fluids. In Ann. Rev. Fluid Mech. 2, Van Dyke & Vincenti, eds., 37-66.

Wolanski, E. J. & Brush, L. M. 1975 Turbulent entrainment across stable density step structures. Tellus 27, 259-268.

Zeman, O. & Tennekes, H. 1977 Parameterization of the turbulent energy budget at the top of the daytime atmospheric boundary layer. J. Atmos. Sci. 34, 111-123.

FIGURE CAPTIONS

Fig. 1. The primary (a) and inner (b) annulus in which the screen (d) rotates. Other parts include: (c) central region; (e) plexiglass walls of outer tank; (f) vertical lines on window for timing particle passages (lines on inner wall of primary annulus not visible); (g) salinity probe arm; (h) lasers. Reflections are present at far left and right.

Fig. 2. Computerized output from Exp. #10 as a function of time after onset of screen rotation. (•) screen speed in primary annulus; (▲) laser-height, h_L, estimate of mixed-layer depth in primary annulus; (+) mixed-layer height estimate in inner annulus which was stirred at intervals; (x) mean mixed-layer speed in primary annulus.

Fig. 3. Momentum-balance estimates of the screen drag coefficient, C_{DS} as a function of Reynolds number $h\bar{v}/\nu$. (x) rough screen, 2LS experiments; (+) rough screen, SOL experiments; (o) smooth screen. Smooth-surface drag-coefficient curve shown obeys (11).

Fig. 4. Direct measurements of $|\Delta v|/\bar{v}$ as a function of $w_e(h/\nu\bar{v})^{\frac{1}{2}}$ from Exp.#15 (x), #16 (•), and #17 (+). In #15 and #17 the screen speed increased in steps; in #16 it decreased in steps.

Fig. 5. Temperature profiles from Exp. #1 at indicated times. Horizontal line segments denote values of h_L at time of traverse of thermocouple. Traverses were upward at 1.2 cm s^{-1}.

Fig. 6. Temperature profiles from Exp. #2. See Fig. 5 caption for further details.

Fig. 7. Density profiles from Exp. #16 at indicated times. Horizontal line segments denote h_L at the respective times. Traverses were upward at from 1-3 cm s^{-1}.

Fig. 8. Density profiles from Exp. #17. See also Fig. 7 caption.

Fig. 9. Theoretical interfacial slopes, s (see (14)) versus sampled slopes in primary annulus, $\partial h_1/\partial r \simeq \partial h_2/\partial r$.

Fig. 10. Vector entrainment diagram indicating net outward entrainment velocity, $\underset{\sim}{V}_e$; vertical entrainment rate, w_e; and horizontal entrainment rate, u_e.

Fig. 11. Experimentally determined entrainment diagram of w_e/u_* versus R_T, using the well-mixed depth h as length scale. Printed values of R_v are encircled for experiments using temperature stratification in the primary annulus; enclosed in rectangles for the 2LS using kaolin; underlined for the inner annulus data using salt in the 2LS; unadorned for the primary annulus data using salt in the 2LS. Sloping lines obey (16a). The KPA data swath is only approximately placed since their length scale may have been $\bar{h}$.

Fig. 12. Entrainment diagram from numerical simulation, using (16c), of a particular KP experiment (curve); and for numerical simulation of 5 KPA experiments (dots). The (plus) and (square) symbols represent the respective KP and KPA experimental results.

Fig. 13. Entrainment diagram using only $\Delta v|_1$ as velocity scale, for the 2LS. Present results (dots, except I=inner-annulus results, K=kaolin results). Comparison is made with results of Ellison & Turner (1959), Lofquist (1960) and Moore & Long (1971).

Fig. A1. Numerical model results, neglecting any gravity-wave momentum transport above $z=h_2$, of $|\Delta v|_1 \bar{v}$ versus $w_e(h_2\bar{v})^{\frac{1}{2}}$ in simulation of Exp. #16 (solid-line path) and #17 (dashed-line path). Letters denote results occurring during designated periods in Table 1. Along either path time progresses in the direction of the arrows.

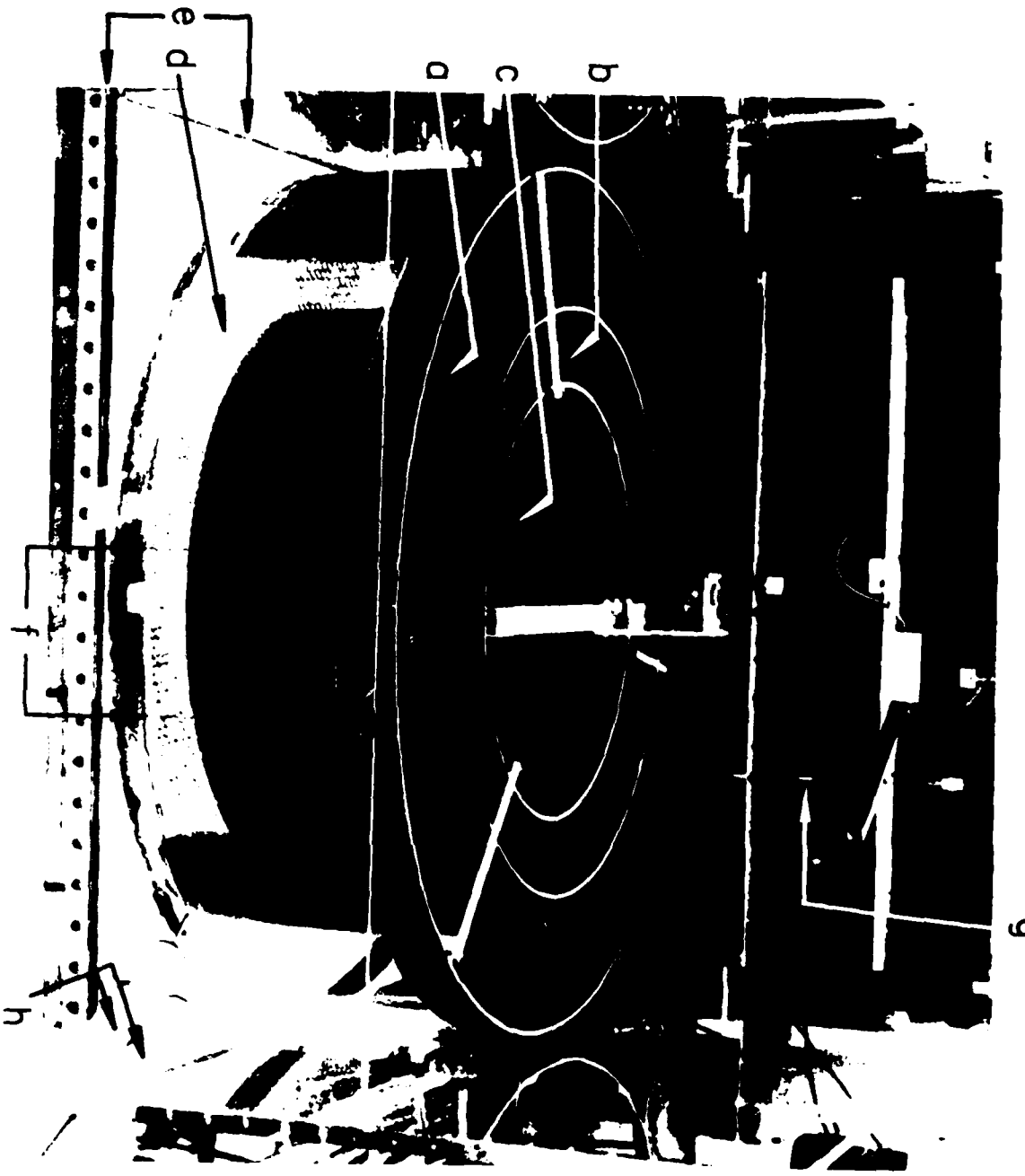

Fig. 1

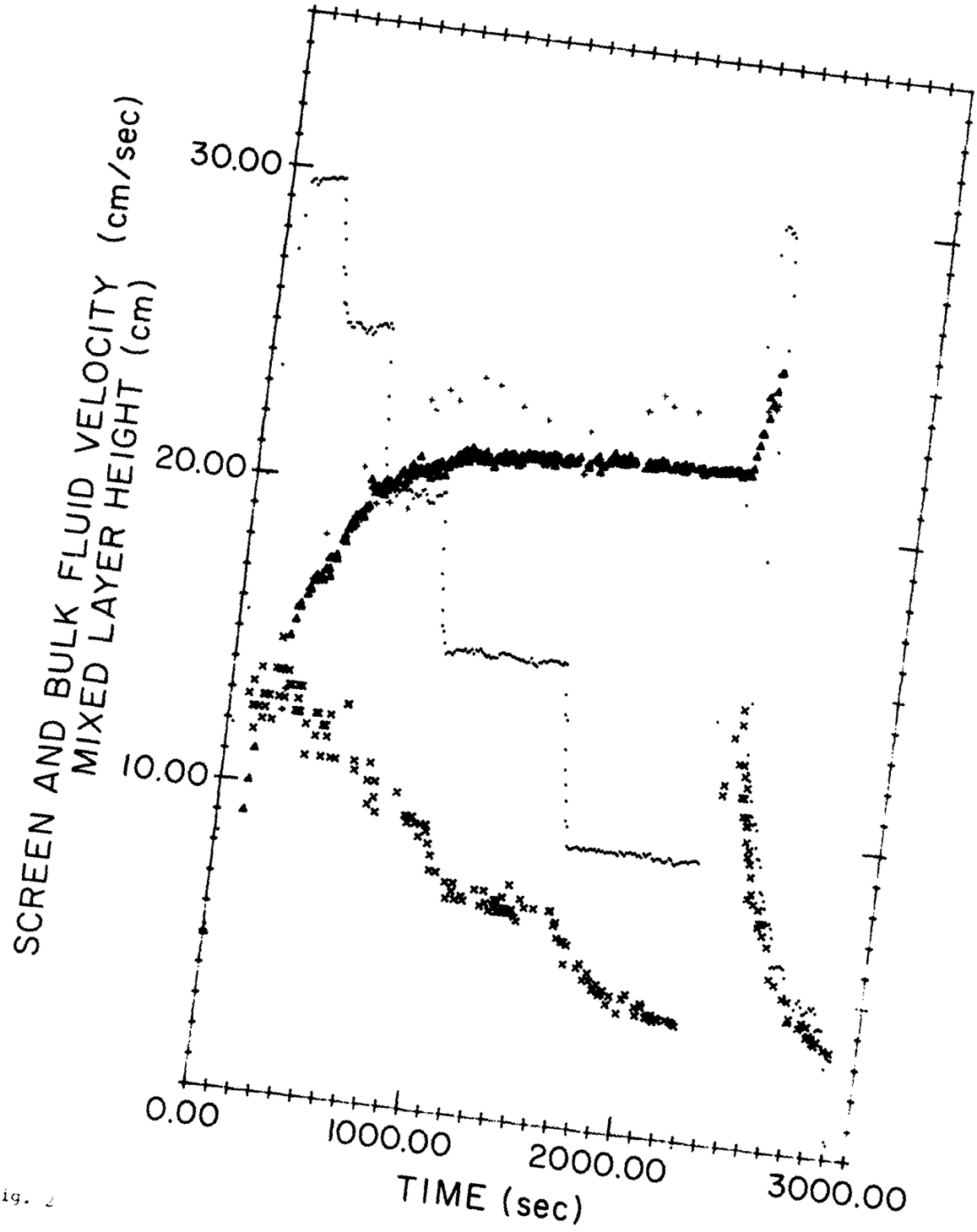
SCREEN AND BULK FLUID VELOCITY (cm/sec)
MIXED LAYER HEIGHT (cm)
30.00
20.00
10.00
0.00
1000.00
2000.00
3000.00
TIME (sec)

Fig. 2

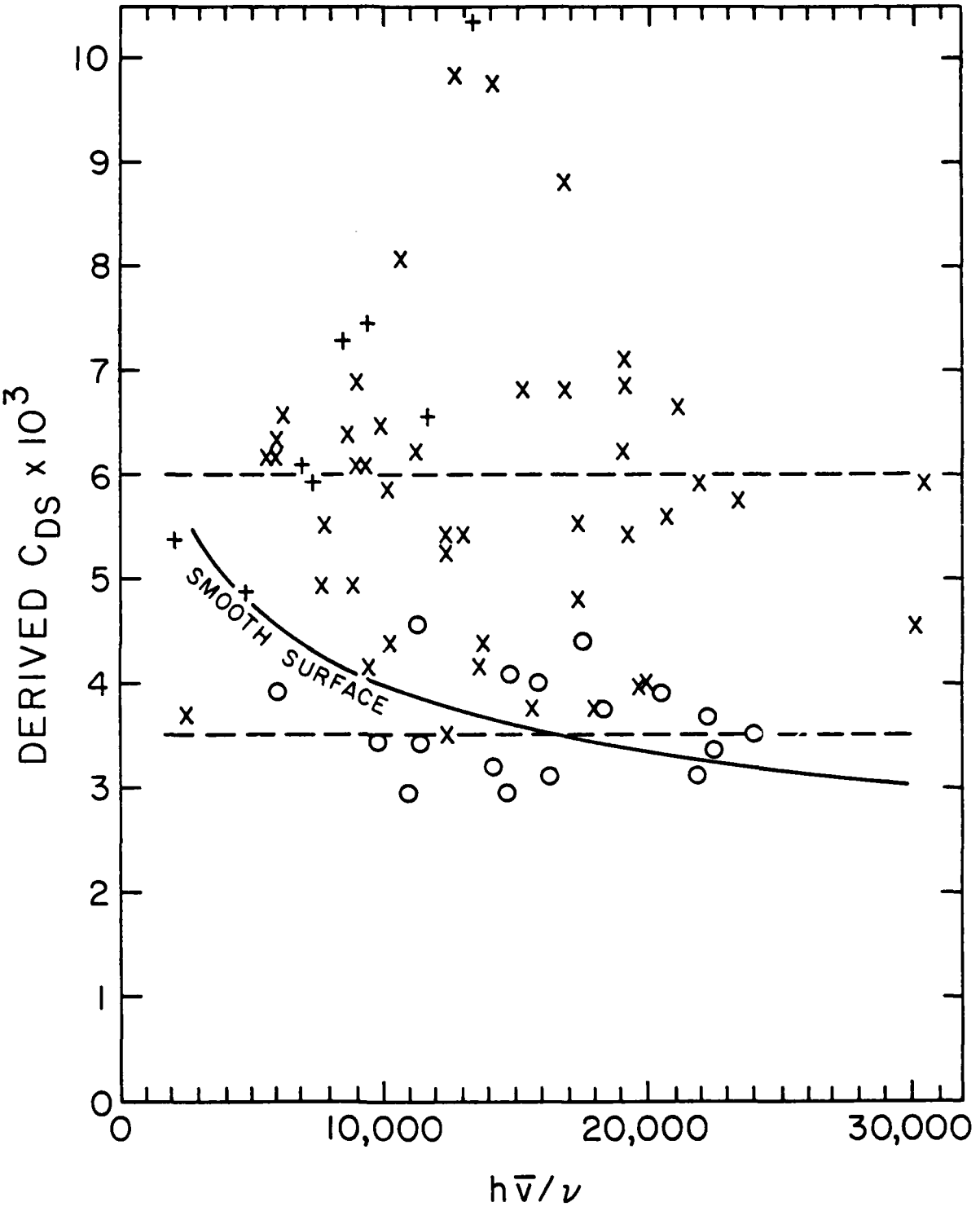
DERIVED $C_{DS} \times 10^3$
10
9
8
7
6
5
4
3
2
1
0
0
10,000
20,000
30,000
$h\bar{\nu}/\nu$
SMOOTH SURFACE

Fig. 3

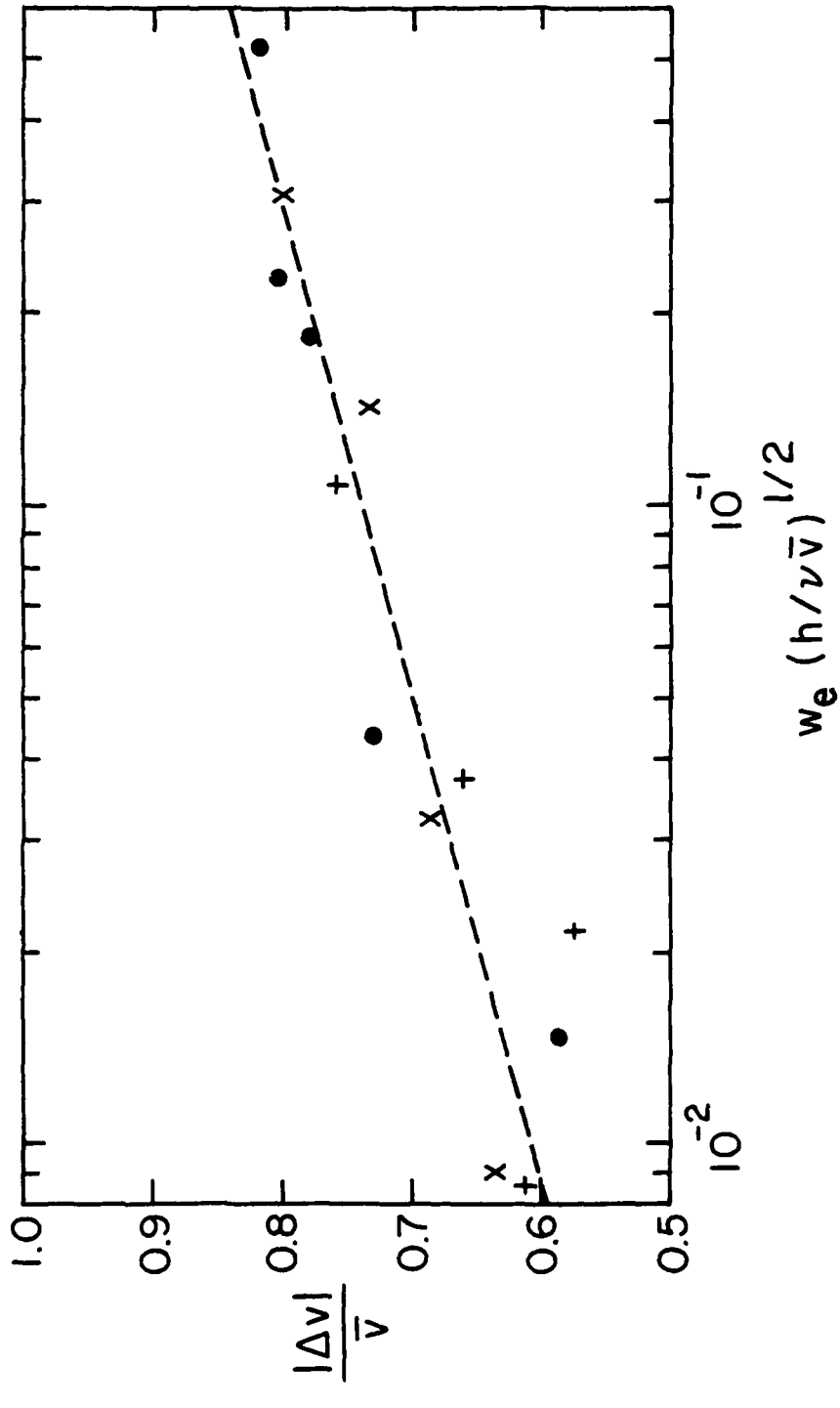

Fig. 4

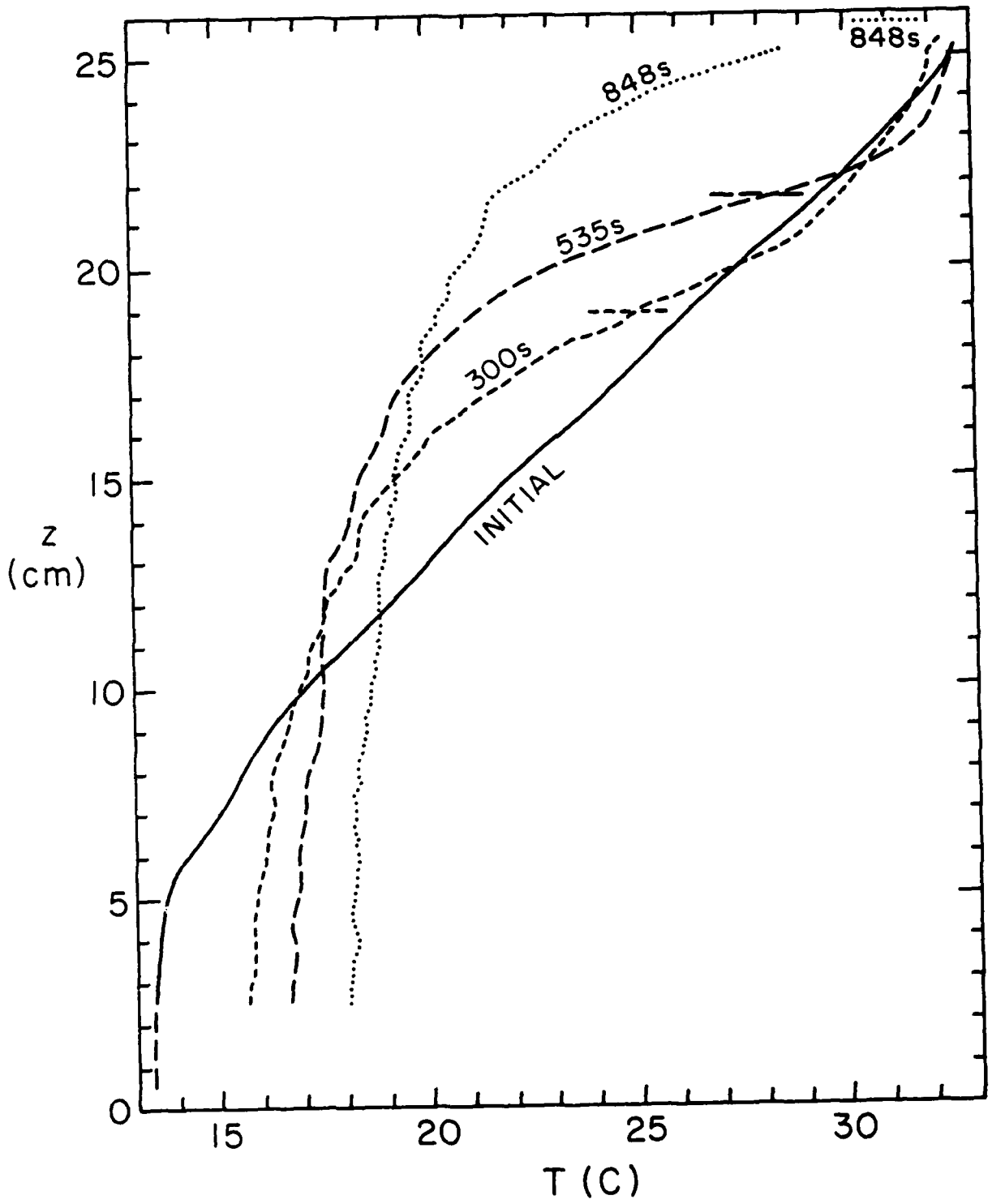

Fig. 5

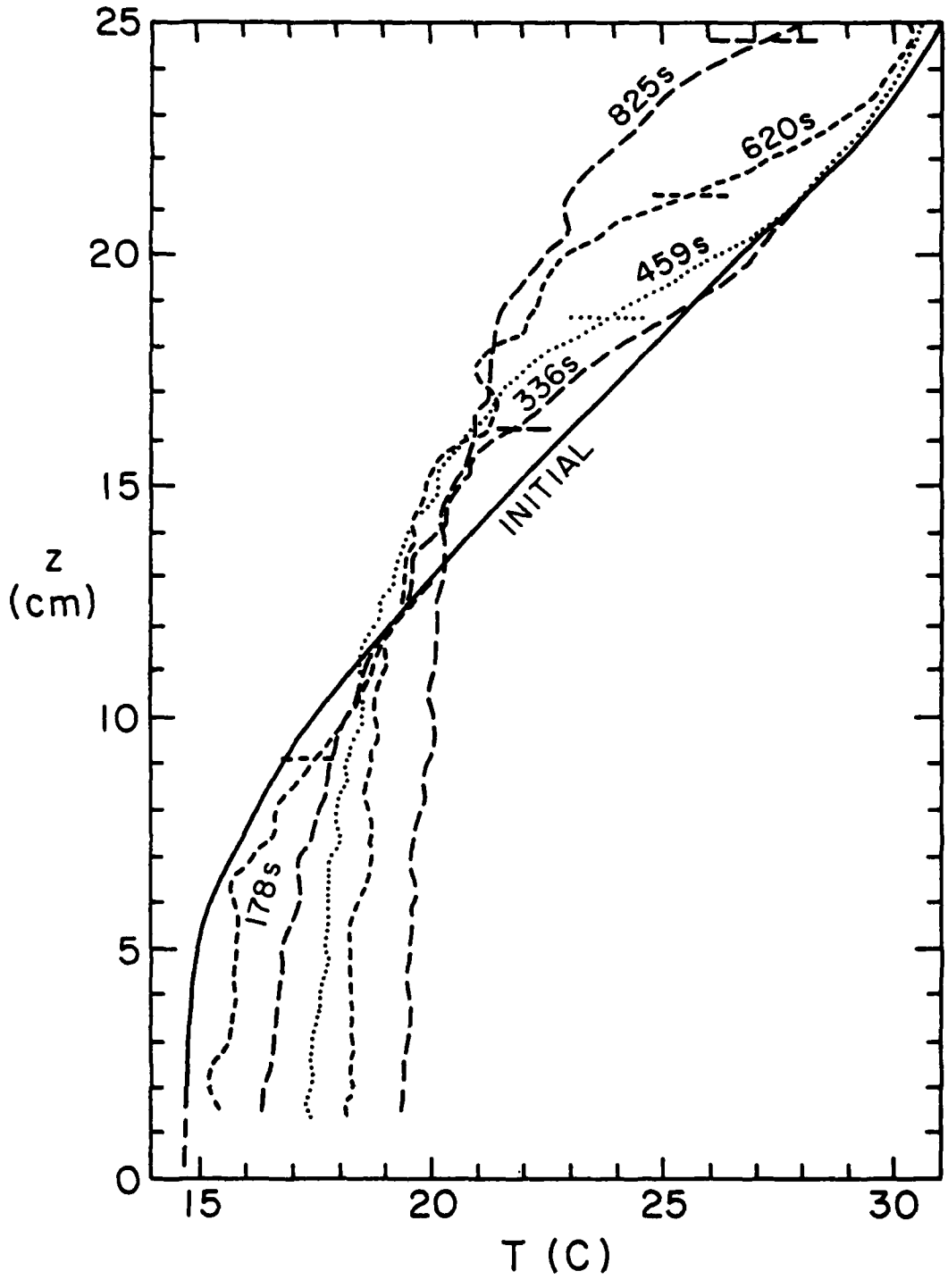
25
20
15
10
5
0
z
(cm)
15
20
25
30
T (C)
825s
620s
459s
336s
178s
INITIAL

Fig. 6

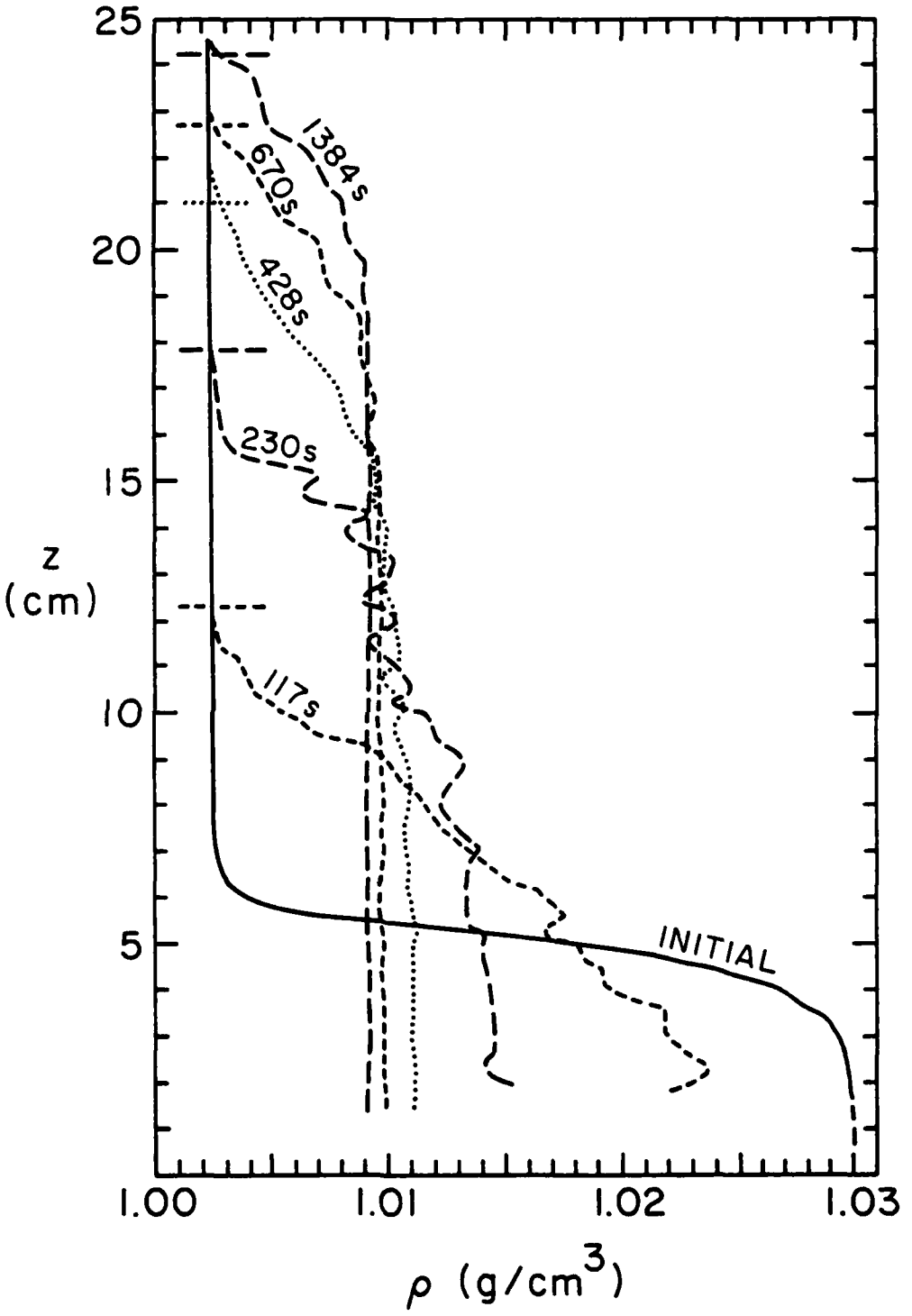
25
20
15
10
5
z
(cm)
1384s
670s
428s
230s
117s
INITIAL
1.00
1.01
1.02
1.03
ρ (g/cm3)

Fig. 7

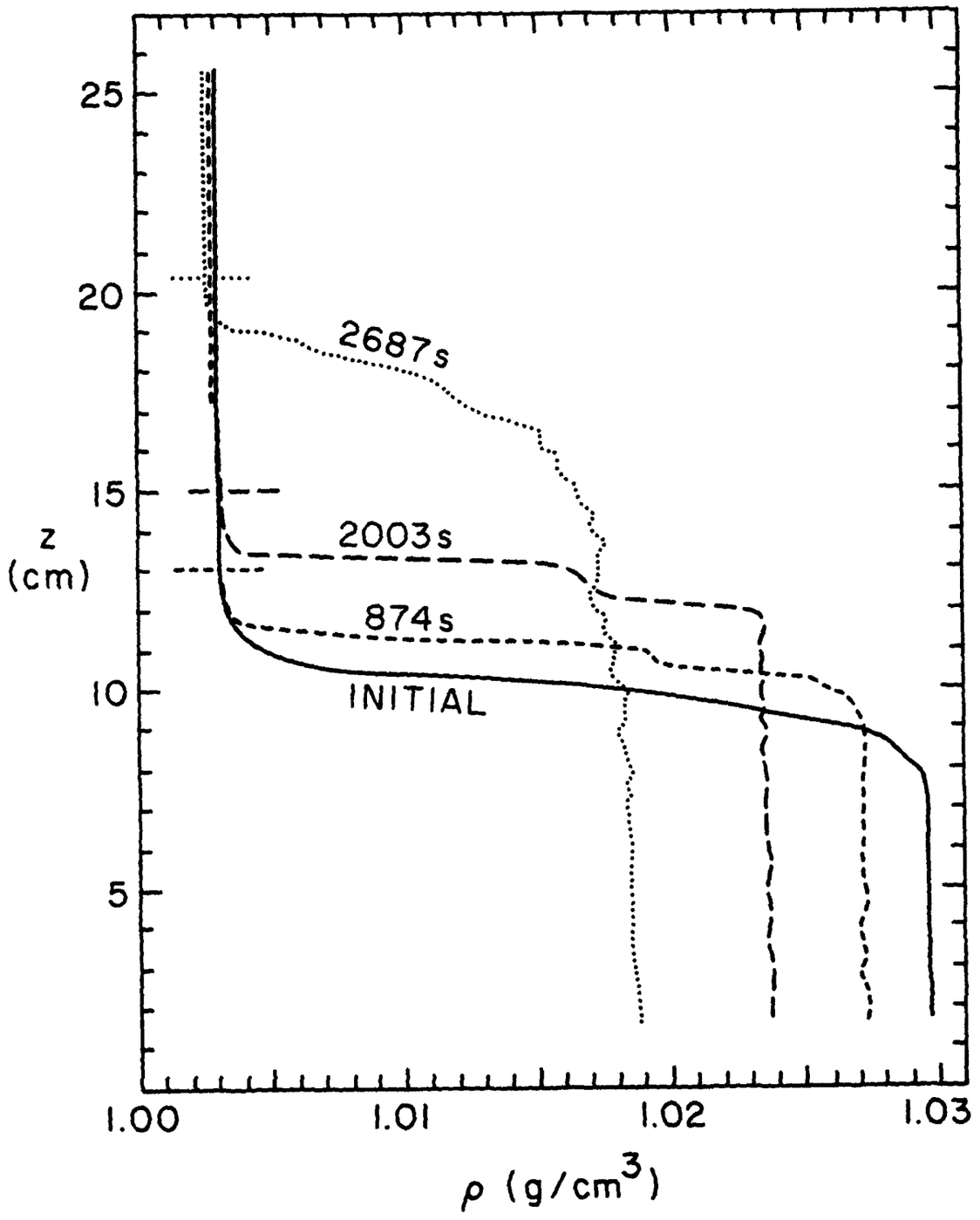
25
20
15
10
5
z
(cm)
2687s
2003s
874s
INITIAL
1.00
1.01
1.02
1.03
ρ (g/cm³)

Fig. 8

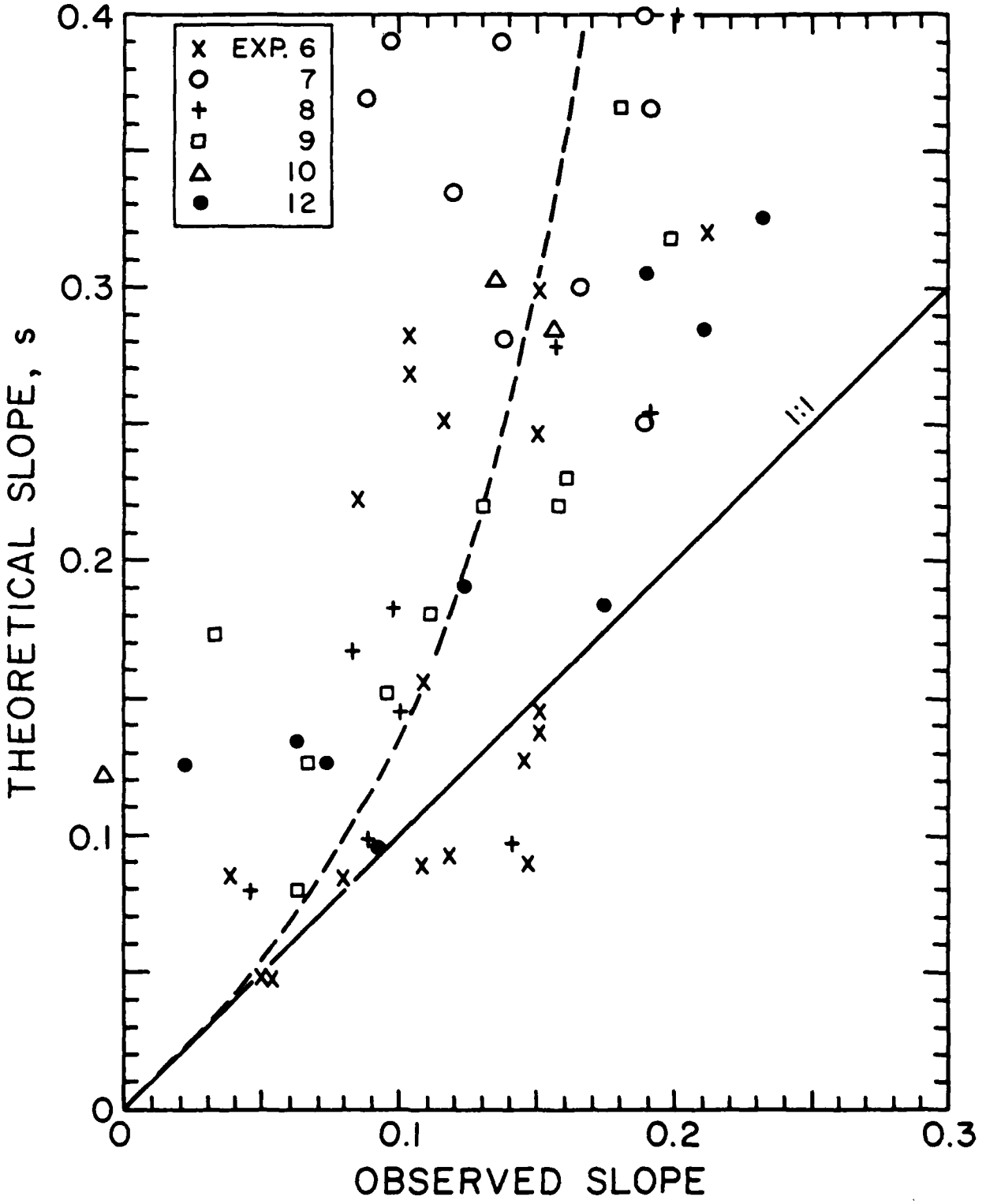
EXP. 6
7
8
9
10
12
1:1
THEORETICAL SLOPE, s
OBSERVED SLOPE
0
0.1
0.2
0.3
0.4

Fig. 9

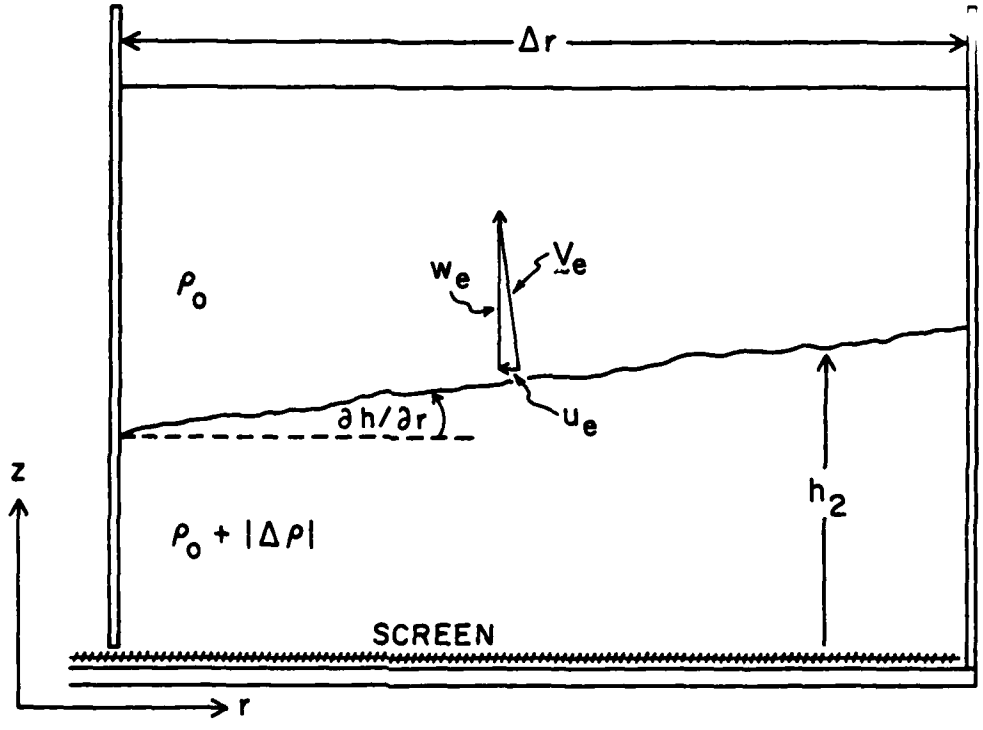
Δr
ρ_0
w_e
V_e
u_e
$\partial h/\partial r$
h_2
z
$\rho_0 + |\Delta\rho|$
SCREEN
r

Fig. 10

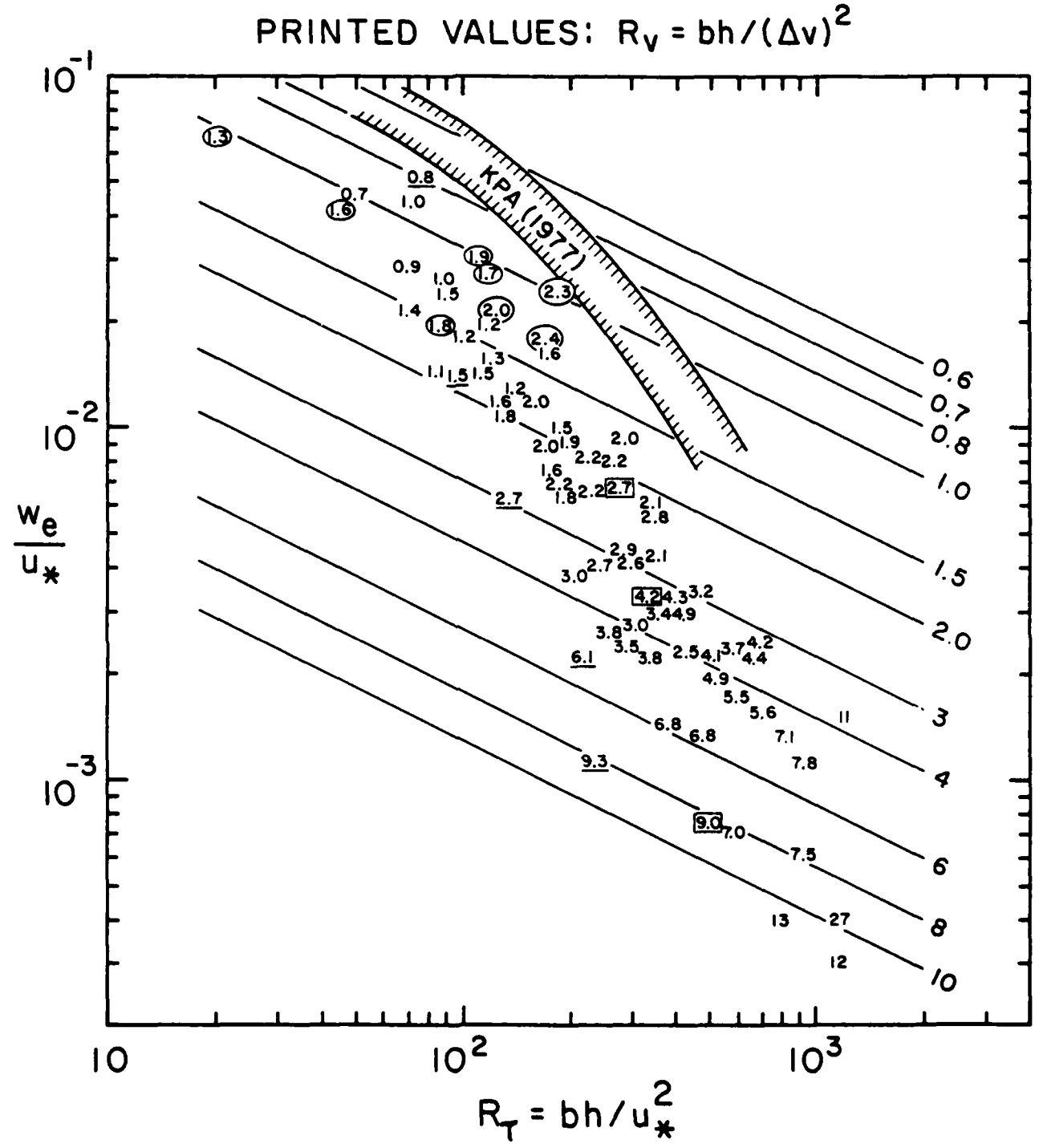
PRINTED VALUES: $R_V = bh/(\Delta v)^2$
KPA (1977)
10^{-1}
10^{-2}
10^{-3}
$\frac{w_e}{u_*}$
10
10^2
10^3
$R_T = bh/u_*^2$
0.6
0.7
0.8
1.0
1.5
2.0
3
4
6
8
10

Fig. 11

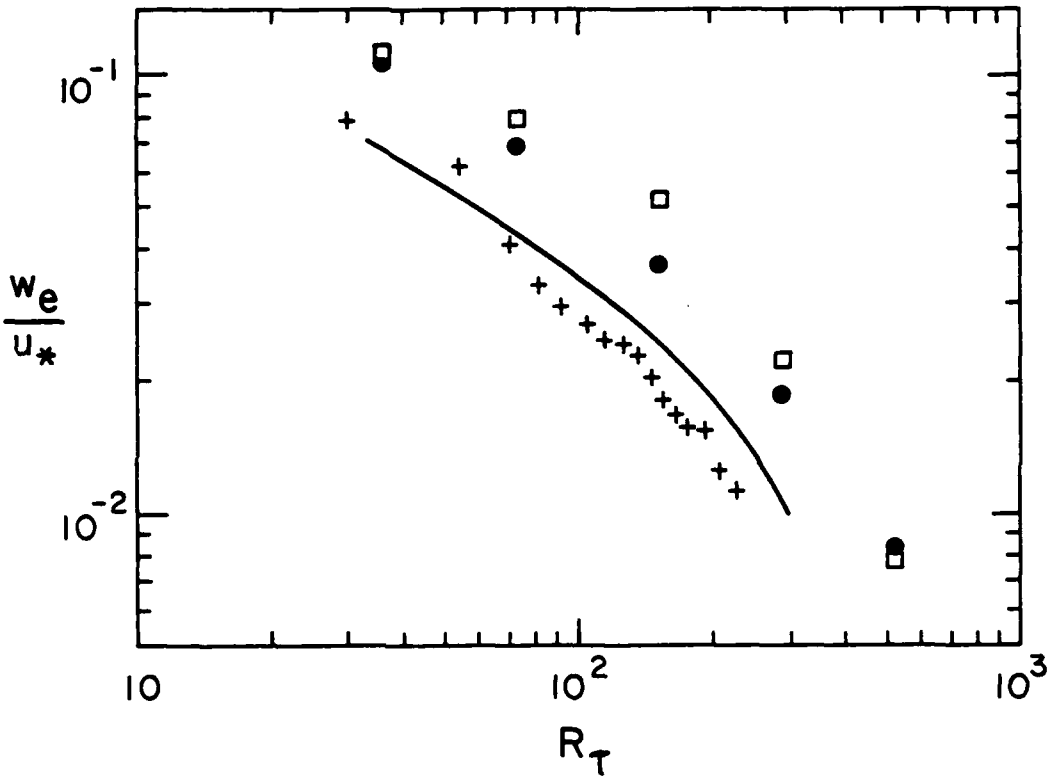

Fig. 12

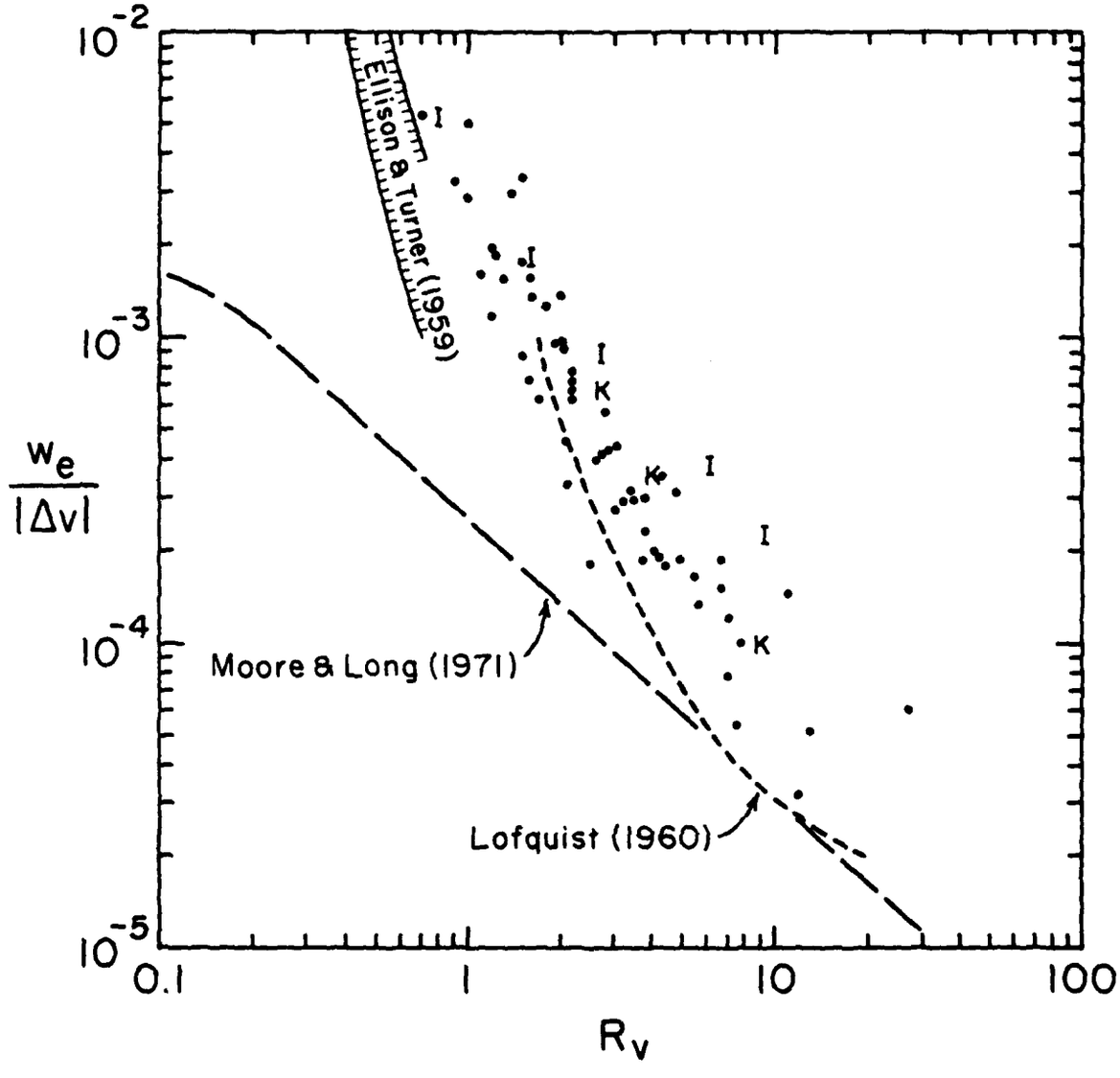
10^{-2}
10^{-3}
10^{-4}
10^{-5}
$\frac{w_e}{|\Delta v|}$
Ellison & Turner (1959)
Moore & Long (1971)
Lofquist (1960)
I
K
0.1
1
10
100
R_v

Fig. 13

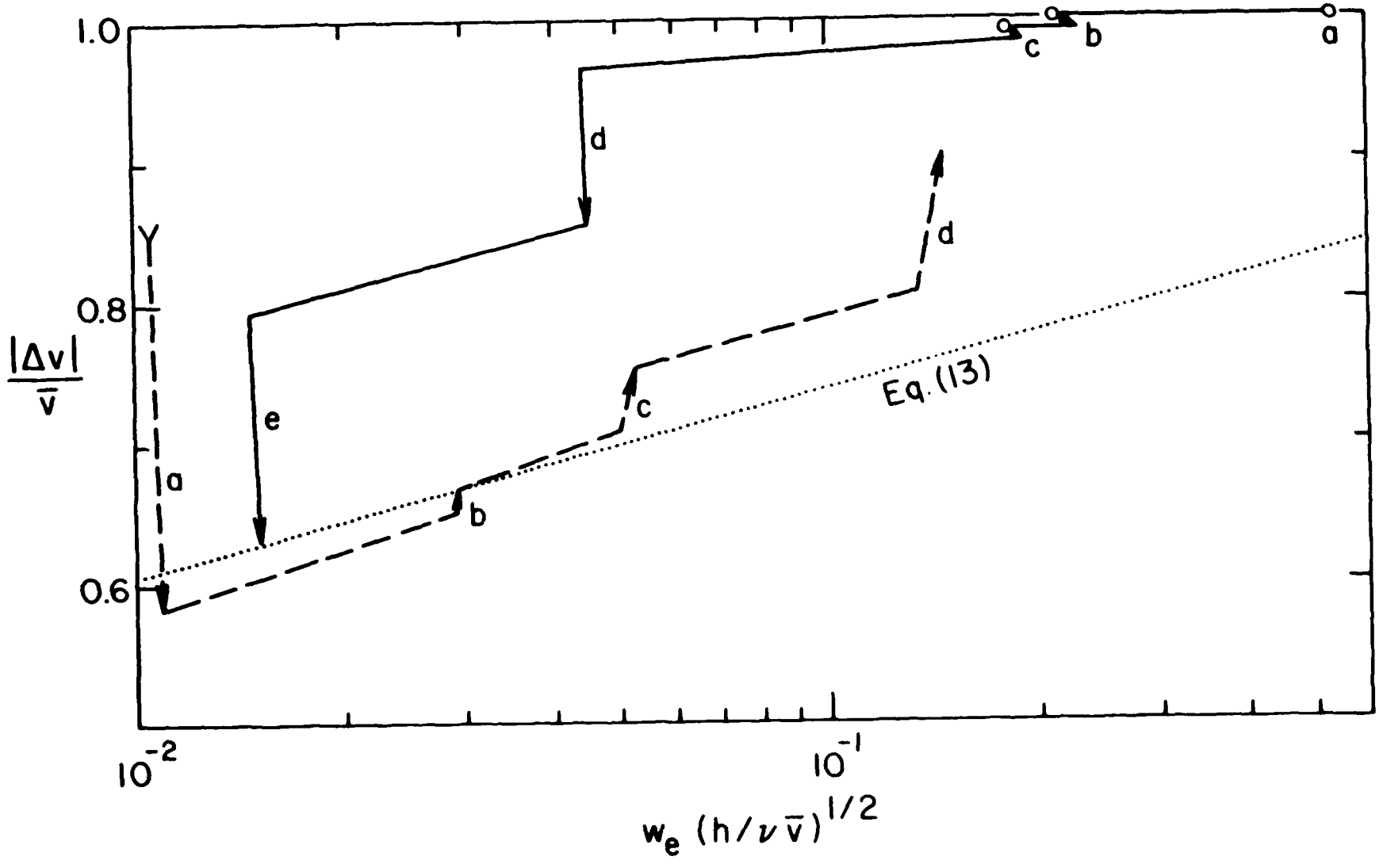

Fig. A1

54

DISTRIBUTION LIST

[illegible] Center
[illegible]
[illegible], [illegible] 20314 [illegible]

Pr[illegible]
U.S. Naval [illegible]
Engineering [illegible]
Ann[illegible], [illegible]

Library
U.S. Naval [illegible]
Annap[illegible]lis, [illegible]

Tech[illegible]
David W. Taylor [illegible] Research
 and [illegible]
Ann[illegible]
Ann[illegible], [illegible]

Profe[illegible]
The [illegible]
Department [illegible]
Ann Ar[illegible], [illegible]

Professor [illegible]
The [illegible]
Department [illegible]
 and Marine [illegible]
Ann Arb[illegible], MI [illegible]

Office of Naval Resear[illegible]
Code 2008
800 N. Quincy Street
Arlington, VA [illegible]

Office of Naval Research
Code [illegible]
800 N. Quincy Street
Arlington, VA [illegible] [illegible]copies

Office of Naval Research
Code [illegible]
800 N. Quincy Street
Arlington, VA [illegible]

NASA Scientific and Technical
 Information Facility
P. O. Box [illegible]
Baltimore/Washington International
 Airport
Maryland [illegible]

Professor Paul M. [illegible]
University of California
Department of Mechanical Engineering
Berkeley, CA [illegible]

Librarian
University of California
Department of Naval Architecture
Berkeley, CA [illegible]

Professor John V. Wehausen
University of California
Department of Naval Architecture
Berkeley, CA [illegible]

Library
David W. Taylor Naval Ship Research
 and Development Center
Code 522.1
Bethesda, MD 20084

Mr. Justin H. McCarthy, Jr.
David W. Taylor Naval Ship Research
 and Development Center
Code 1552
Bethesda, MD 20084

Dr. William B. Morgan
David W. Taylor Naval Ship Research
 and Development Center
Code 1540
Bethesda, MD 20084

Director
Office of Naval Research Eastern/Central
Building 114, Section D Regional Office
666 Summer Street
Boston, MA 02210

Library
Naval Weapons Center
China Lake, CA 93555

Technical Library
Naval Surface Weapons Center
Dahlgren Laboratory
Dahlgren, VA 22448

Technical Documents Center
Army Mobility Equipment Research & Development Center
Building 315
Fort Belvoir, VA 22060

Technical Library
Webb Institute of Naval Architecture
Glen Cove, NY 11542

Dr. J. P. Breslin
Stevens Institute of Technology
Davidson Laboratory
Castle Point Station
Hoboken, NJ 07030

Professor Louis Landweber
The University of Iowa
Institute of Hydraulic Research
Iowa City, IA 52242

R. E. Gibson Library
The Johns Hopkins University
Applied Physics Laboratory
Johns Hopkins Road
Laurel, MD 20810

Lorenz G. Straub Library
University of Minnesota
St. Anthony Falls Hydraulic Laboratory
Minneapolis, MN 55414

Library
Naval Postgraduate School
Monterey, CA 93940

Technical Library
Naval Underwater Systems Center
Newport, RI 02840

Engineering Societies Library
345 East 47th Street
New York, NY 10017

The Society of Naval Architects and
Marine Engineers
One World Trade Center, Suite 1369
New York, NY 10048

Technical Library
Naval Coastal System Laboratory
Panama City, FL 32401

Professor Theodore Y. Wu
California Institute of Technology
Engineering Science Department
Pasadena, CA 91125

Director
Office of Naval Research Western Regional
1030 E. Green Street Office
Pasadena, CA 91101

Technical Library
Naval Ship Engineering Center
Philadelphia Division
Philadelphia, PA 19112

Army Research Office
P. O. Box 12211
Research Triangle Park, NC 27709

Editor
Applied Mechanics Review
Southwest Research Institute
8500 Culebra Road
San Antonio, TX 78206

Technical Library
Naval Ocean Systems Center
San Diego, CA 92152

ONR Scientific Liaison Group
American Embassy - Room A-407
APO San Francisco 96503

Librarian
Naval Surface Weapons Center
White Oak Laboratory
Silver Spring, MD 20910

Defense Research and Development Attache
Australian Embassy
1601 Massachusetts Avenue, NW
Washington, DC 20036

Oceanographer of the Navy
200 Stovall Street
Alexandria, VA 22332

Office of Naval Research
Code 481
800 N. Quincy Street
Arlington, VA 22217

Professor Richard W. Miksad
The University of Texas at Austin
Department of Civil Engineering
Austin, TX 78712

Dr. Robert R. Long
The Johns Hopkins University
Department of Earth and
Planetary Sciences
Baltimore, MD 21218

Professor Owen M. Phillips
The Johns Hopkins University
Department of Earth and
Planetary Sciences
Baltimore, MD 21218

Professor C. C. Mei
Massachusetts Institute of Technology
Department of Civil Engineering
Cambridge, MA 02139

Professor David J. Benney
Massachusetts Institute of Technology
Department of Mathematics
Cambridge, MA 02139

Professor E. Mollo-Christensen
Massachusetts Institute of Technology
Department of Meteorology
Room 54-1722
Cambridge, MA 02139

Professor Justin E. Kerwin
Massachusetts Institute of Technology
Department of Ocean Engineering
Cambridge, MA 02139

Professor Phillip Mandel
Massachusetts Institute of Technology
Department of Ocean Engineering
Cambridge, MA 02139

Professor J. Nicholas Newman
Massachusetts Institute of Technology
Department of Ocean Engineering
Room 5-324A
Cambridge, MA 02139

Professor Francis Noblesse
Massachusetts Institute of Technology
Department of Ocean Engineering
Cambridge, MA 02139

Professor Ronald W. Yeung
Massachusetts Institute of Technology
Department of Ocean Engineering
Cambridge, MA 02139

Professor J. M. Burgers
University of Maryland
Institute of Fluid Dynamics
and Applied Mathematics
College Park, MD 20742

Professor S. I. Pai
University of Maryland
Institute of Fluid Dynamics
and Applied Mathematics
College Park, MD 20742

Computation and Analyses Laboratory
Naval Surface Weapons Center
Dahlgren Laboratory
Dahlgren, VA 22418

Dr. Robert K. -C. Chan
JAYCOR
1401 Camino Del Mar
Del Mar, CA 92014

Professor K. E. Shuler
University of California, San Diego
Department of Chemistry
La Jolla, CA 92093

Professor John W. Miles
University of California, San Diego
Institute of Geophysics and
Planetary Physics, A-025
La Jolla, CA 92093

Dr. E. W. Montroll
Physical Dynamics, Inc.
P. O. Box 556
La Jolla, CA 92038

Director
Scripps Institute of Oceanography
University of California
La Jolla, CA 92037

Dr. Steven A. Orszag
Cambridge Hydrodynamics, Inc.
54 Baskin Road
Lexington, MA 02173

Dr. Steven C. Crow
President, Poseidon Research
11777 San Vicente Blvd., Suite 641
Los Angeles, CA 90049

Professor Frederick K. Browand
University of Southern California
University Park
Department of Aerospace Engineering
Los Angeles, CA 90007

Professor John Laufer
University of Southern California
University Park
Department of Aerospace Engineering
Los Angeles, CA 90007

Professor T. N. Stevenson
University of Manchester
Department of the Mechanics of Fluids
Manchester M13 9PL, England

Professor Jin Wu
University of Delaware
College of Marine Studies
Newark, DE 19711

Professor R. C. MacCamy
Carnegie Institute of Technology
Department of Mathematics
Pittsburgh, PA 15213

Professor Norman J. Zabusky
University of Pittsburgh
Department of Mathematics and Statistics
Pittsburgh, PA 15260

Dr. Harvey Segur
Aeronautical Research Associates
of Princeton, Inc.
50 Washington Road
Princeton, NJ 08540

Professor J. T. C. Liu
Brown University
Division of Engineering
Providence, RI 02912

Professor C. H. Su
Brown University
Division of Applied Mathematics
Providence, RI 02912

Dr. Jack W. Hoyt
Naval Ocean Systems Center
Code 2501
San Diego, CA 92152

Professor Milton Van Dyke
Stanford University
Department of Aeronautics
and Astronautics
Stanford, CA 94305

Professor J. F. Thompson
Mississippi State University
Department of Aerophysics and
Aerospace Engineering
State College, MS 39762

Professor Richard L. Pfeffer
Florida State University
Geophysical Fluid Dynamics Institute
Tallahassee, FL 32306

Professor Ruby E. Krishnamurti
Florida State University
Department of Oceanography
Tallahassee, FL 32306

Professor Timothy W. Kao
The Catholic University of America
Department of Civil Engineering
Washington, DC 20064

Librarian Station 5-2
Coast Guard Headquarters
NASSIF Building
400 Seventh Street, SW
Washington, DC 20591

Library of Congress
Science and Technology Division
Washington, DC 20540

Dr. A. L. Slafkosky
Scientific Advisor
Commandant of the Marine Corps
Code AX
Washington, DC 20380

Maritime Administration
Office of Maritime Technology
14th & E Streets, NW
Washington, DC 20230

Maritime Administration
Division of Naval Architecture
14th & E Streets, NW
Washington, DC 20230

Dr. G. Kulin
National Bureau of Standards
Mechanics Section
Washington, DC 20234

Naval Research Laboratory
Code 2627
Washington, DC 20375 6 copies

Library
Naval Sea Systems Command
Code 09GS
Washington, DC 20362

Mr. Thomas E. Peirce
Naval Sea Systems Command
Code 03512
Washington, DC 20362

Mr. M. Stanley
NORDA Code 540
Bay St. Louis, MS 39527

Mr. Stanley W. Doroff
Mechanical Technology, Inc.
2731 Prosperity Avenue
Fairfax, VA 22031

Dr. Charles Watkins
Head, Mechanical Engineering Department
Howard University
Washington, DC 20059

Mr. D. Farmer
Naval Ocean Research and
Development Activity
Code 332
NSTL Station, MS 39522

Professor Hsien-Ping Pao
The Catholic University of America
Department of Civil Engineering
Washington, DC 20064

Commander
Naval Oceanographic Office
Washington, DC 20373

Dr. J. O. Elliot
Naval Research Laboratory
Code 8310
Washington, DC 20375

Naval Research Laboratory
Code 8340
Washington, DC 20375

Naval Ship Engineering Center
Code 6110
Washington, DC 20362

Naval Ship Engineering Center
Code 6114
Washington, DC 20362

Naval Ship Engineering Center
Code 6136
Washington, DC 20362

Dr. Gary S. Deem
Bell Telephone Laboratories, Inc.
1 Whippany Road
Whippany, NJ 07981

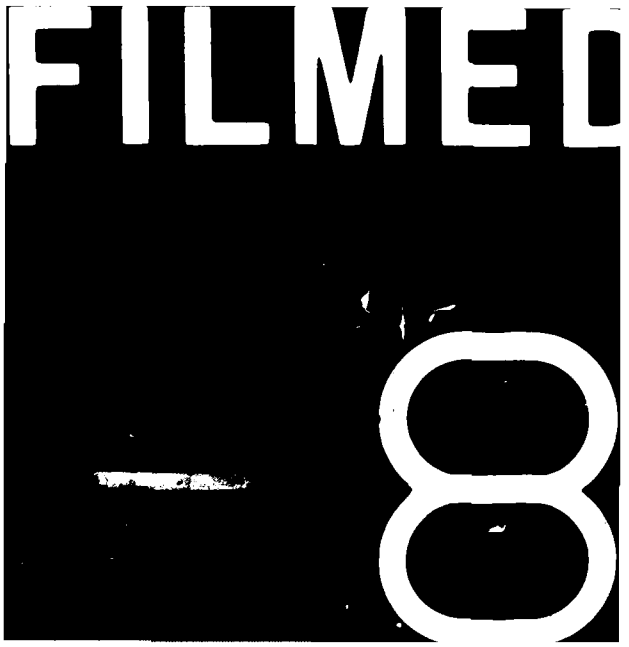
FILMED
8